Binucleating Ligand Structural Effects on (μ-Peroxo)- and Bis(μ-oxo)dicopper Complex Formation and Decay: Competition between Arene Hydroxylation and Aliphatic C−H Bond Activation

Samiran Mahapatra,[†] Susan Kaderli,[‡] Antoni Llobet,[‡] Yorck-Michael Neuhold,[‡] Tania Palanché,[‡] Jason A. Halfen,[†] Victor G. Young, Jr.,[†] Thomas A. Kaden,[‡] Lawrence Que, Jr.,[†] Andreas D. Zuberbühler,*[,‡] and William B. Tolman*[,†]

Department of Chemistry and Center for Metals in Biocatalysis, University of Minnesota, 207 Pleasant Street SE, Minneapolis, Minnesota 55455, and Institut für Anorganische Chemie, University of Basel, Spitalstrasse 51, CH-4056 Basel, Switzerland

Received June 12, 1997[⊗]

The reactivity of dicopper(I) complexes of the ligands α,α′-bis(4,7-diisopropyl-1,4,7-triazacyclononan-1-yl)-*p*- and *m*-xylene (*p*- and *m*-XYL^{iPr4}) with dioxygen was examined by spectroscopic and rapid stopped-flow kinetics methods. Only bis(μ-oxo)dicopper(III) core formation was observed with *p*-XYL^{iPr4}, but both (μ-η^2:η^2-peroxo)-dicopper(II) and bis(μ-oxo)dicopper(III) species were generated in the *m*-XYL^{iPr4} case, their relative proportions being dependent on the solvent, concentration of the dicopper(I) precursor, and temperature. Subsequent decomposition under conditions that favored bis(μ-oxo) core formation resulted in oxidative N-dealkylation of isopropyl groups, whereas μ-η^2:η^2-peroxo decay led to the product resulting from hydroxylation of the bridging arene, [(*m*-XYL^{iPr4}-O)Cu$_2$(μ-OH)](SbF$_6$)$_2$. Evidence from kinetics studies, decomposition product analyses, and comparison to the chemistry exhibited by complexes of other substituted 1,4,7-triazacyclonane ligands support a model for the oxygenation of the *m*-XYL^{iPr4} compound involving initial, essentially rate-limiting 1:1 Cu:O$_2$ adduct formation followed by partitioning between intra- and intermolecular pathways. At low temperature and high starting material concentrations, the latter route that yields tetranuclear "dimer-of-dimer" species and/or higher order oligomers with bis(μ-oxo) cores is favored, while at higher temperatures and dilution, intramolecular reaction predominates to afford a (peroxo)dicopper(II) species. The course of the subsequent decompositions of these oxygenated products correlates with their proposed formulations. Thus, analysis of final products and kinetics data, including with selectively deuterated compounds, showed that N-dealkylation arises from the high-nuclearity bis(μ-oxo) species and arene hydroxylation occurs upon decay of the intramolecular peroxo complex. Geometric rationales for the divergent oxygenation and decomposition reactions supported by *p*- and *m*-XYL^{iPr4} are proposed.

Introduction

An important goal in bioinorganic chemistry research is to understand in detail the mechanisms of copper monooxygenases, in which active sites of varying copper ion nuclearity use atmospheric dioxygen to regio- and stereoselectively hydroxylate hydrocarbons.[1,2] Notable examples include tyrosinase (Tyr), which employs a coupled dicopper site to hydroxylate monophenols and convert the resulting *o*-catechols to *o*-quinones,[2,3] dopamine β-monooxygenase (DβM)[1] and peptidylglycine α-amidating monooxygenase (PAM),[1,4] which use a single copper center to hydroxylate the benzylic position of dopamine and the α-carbon of glycine extended peptides, respectively, and particulate methane monooxygenase (pMMO), which has been suggested to use a multicopper cluster of poorly defined structure to convert methane to methanol.[5] Proposed mechanisms for these and other copper monooxygenases have in common dioxygen binding to reduced (Cu$^{I}_n$) sites to generate a Cu$_n$−O$_2$ adduct that undergoes O−O bond scission either prior to or concomitant with attack on substrate. The hypotheses differ considerably, however, with regard to the nature of the Cu$_n$−O$_2$ adducts and the sequence and detailed manner by which O−O and substrate C−H bonds are cleaved, among other issues.[1,2] In order to construct a coherent mechanistic view of metallomonooxygenase function, and, by extension, the pathways traversed in other catalytic oxidation systems,[6] clear relationships between the structural features of Cu$_n$−O$_2$ species and their reactivity with hydrocarbons need to be defined.

In efforts to address this research objective, we and others have attempted to characterize in detail synthetic copper−dioxygen complexes through the application of structural,

* Authors to whom correspondence should be addressed. Fax: A.D.Z., +4161-267-1020; W.B.T., 612-624-7029. E-mail: A.D.Z., zuberbuehle@ubaclu.unibas.ch; W.B.T., tolman@chem.umn.edu.

[†] University of Minnesota.

[‡] University of Basel.

[⊗] Abstract published in *Advance ACS Abstracts,* December 15, 1997.

(1) Klinman, J. P. *Chem. Rev.* **1996**, *96*, 2541−2561.

(2) Solomon, E. I.; Sundaram, U. M.; Machonkin, T. E. *Chem. Rev.* **1996**, *96*, 2563−2605.

(3) Sánchez-Ferrer, A.; Rodríguez-López, J. N.; García-Cánovas, F.; García-Carmona, F. *Biochim. Biophys. Acta* **1995**, *1247*, 1−11.

(4) (a) Merkler, D. J.; Kulathila, R.; Young, S. D.; Freeman, J.; Villafranca, J. J. In *Bioinorganic Chemistry of Copper*; Karlin, K. D., Tyeklár, Z., Eds.; Chapman & Hall: New York, 1993; pp 196−209. (b) Prigge, S. T.; Kolhekar, A. S.; Eipper, B. A.; Mains, R. E.; Amzel, L. M. *Science* **1997**, *278*, 1300−1305.

(5) (a) Nguyen, H.-H. T.; Nakagawa, K. H.; Hedman, B.; Elliott, S. J.; Lidstrom, M. E.; Hodgson, K. O.; Chan, S. I. *J. Am. Chem. Soc.* **1996**, *118*, 12766−12776. (b) Nguyen, H.-H. T.; Shiemke, A. K.; Jacobs, S. J.; Hales, B. J.; Lindstrom, M. E.; Chan, S. I. *J. Biol. Chem.* **1994**, *269*, 14995−15005. (c) Elliot, S. J.; Zhu, M.; Tso, L.; Nguyen, H.-H. T.; Yip, J. H.-K.; Chan, S. I. *J. Am. Chem. Soc.* **1997**, *119*, 9949−9955.

(6) (a) Sheldon, R. A.; Kochi, J. K. *Metal-Catalyzed Oxidations of Organic Compounds*; Academic Press: New York, 1981. (b) *The Activation of Dioxygen and Homogeneous Catalytic Oxidation*; Barton, D. H. R., Martell, A. E., Sawyer, D. T., Eds.; Plenum Press: New York, 1993.

S0020-1669(97)00718-0 CCC: $14.00

Scheme 1

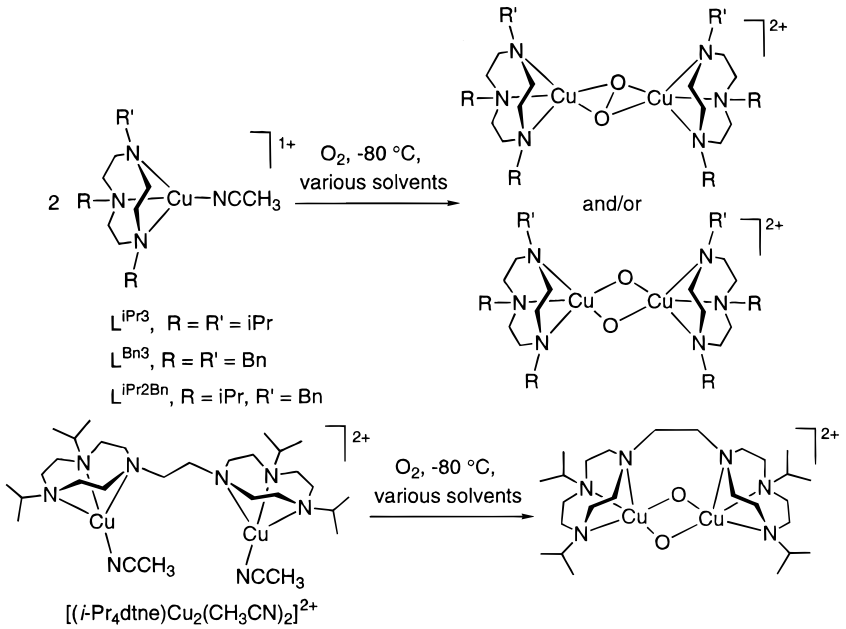

spectroscopic, theoretical, and kinetic/mechanistic methods.[7] Recently, we reported the generation of (μ-η^2:η^2-peroxo)dicopper(II) and/or bis(μ-oxo)dicopper(III) complexes upon low-temperature oxygenation of Cu^I precursors supported by sterically hindered *N*,*N*′,*N*″-trisubstituted 1,4,7-triazacyclononane ligands (L^{R3}; R = isopropyl and/or benzyl; Scheme 1).[8−10] The relative stability of the two isomeric cores was found to depend in a complex manner on the nature of the macrocyclic ligand substituents, the solvent, and the counterions. Thus, for L^{Bn3} and L^{iPr2Bn}, only the contracted (Cu···Cu ≈ 2.8 Å) bis(μ-oxo) core was observed, whereas for L^{iPr3} the bis(μ-oxo) unit formed in THF, the peroxo core predominated in CH_2Cl_2 (Cu···Cu ≈ 3.6 Å, by analogy to structurally characterized cases, including oxyhemocyanin[11]), and both were observed and found to equilibrate with each other in acetone. When the macrocycles were tethered by a short ethyl linker in the binucleating ligand 1,2-bis(4,7-diisopropyl-1,4,7-triaza-1-cyclononyl)ethane (*i*-Pr_4-dtne; Scheme 1), formation of the larger peroxo core was not observed, the bis(μ-oxo) core was induced to bend, and its reactivity was modulated.[12] All of the peroxo and bis(μ-oxo) complexes are thermally unstable and decompose by rate-determining scission of substituent C−H bonds α to the N atom, the net result in the bis(μ-oxo) cases being N-dealkylation through a monooxygenase reaction (eq 1).[13]

$$R_2NCH_2R' + H_2O + [Cu_2(\mu\text{-}O)_2]^{2+} \rightarrow R_2NH + R'CHO + [Cu_2(\mu\text{-}OH)_2]^{2+} \quad (1)$$

In the present work, we extend these studies by examining the copper−dioxygen chemistry of ligands composed of hindered 1,4,7-triazacyclononanes linked by *p*- and *m*-xylyl groups, *p*- and *m*-XYL^{iPr4}. Related *m*-xylyl-bridged ligand systems

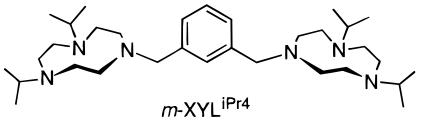

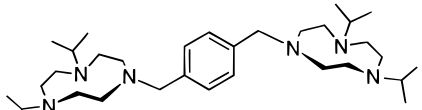

previously had been shown to undergo regiospecific intramolecular arene hydroxylation upon treatment of their dicopper(I) complex precursors with O_2.[14] Detailed mechanistic studies by Karlin et al. using ligands with bis(pyridylmethyl)amine caps implicated the involvement of a (μ-η^2:η^2-peroxo)dicopper

(7) Reviews: (a) Karlin, K. D.; Gultneh, Y. *Prog. Inorg. Chem.* **1987**, *35*, 219−328. (b) Sorrell, T. N. *Tetrahedron* **1989**, *40*, 3−68. (c) Karlin, K. D.; Tyeklár, Z.; Zuberbühler, A. D. In *Bioinorganic Catalysis*; Reedijk, J., Ed.; Marcel Dekker, Inc.: New York, 1993; pp 261−315. (d) Kitajima, N.; Moro-oka, Y. *Chem. Rev.* **1994**, *94*, 737−757. (e) Karlin, K. D.; Tyeklár, Z. *Adv. Inorg. Biochem.* **1994**, *9*, 123−172. (f) Fox, S.; Karlin, K. D. In *Active Oxygen in Biochemistry*; Valentine, J. S., Foote, C. S., Greenberg, A., Liebman, J. F., Eds.; Blackie Academic & Professional, Chapman & Hall: Glasgow, Scotland, 1995; pp 188−231. (g) Karlin, K. D.; Kaderli, S.; Zuberbühler, A. D. *Acc. Chem. Res.* **1997**, *30*, 139−147.

(8) Mahapatra, S.; Halfen, J. A.; Wilkinson, E. C.; Que, L., Jr.; Tolman, W. B. *J. Am. Chem. Soc.* **1994**, *116*, 9785−9786.

(9) (a) Halfen, J. A.; Mahapatra, S.; Wilkinson, E. C.; Kaderli, S.; Young, V. G., Jr.; Que, L., Jr.; Zuberbühler, A. D.; Tolman, W. B. *Science* **1996**, *271*, 1397−1400. (b) Mahapatra, S.; Halfen, J. A.; Wilkinson, E. C.; Pan, G.; Wang, X.; Young, V. G., Jr.; Cramer, C. J.; Que, L., Jr.; Tolman, W. B. *J. Am. Chem. Soc.* **1996**, *118*, 11555−11574.

(10) Tolman, W. B. *Acc. Chem. Res.* **1997**, *30*, 227−237.

(11) (a) Kitajima, N.; Fujisawa, K.; Fujimoto, C.; Moro-oka, Y.; Hashimoto, S.; Kitagawa, T.; Toriumi, K.; Tatsumi, K.; Nakamura, A. *J. Am. Chem. Soc.* **1992**, *114*, 1277−1291. (b) Magnus, K. A.; Hazes, B.; Ton-That, H.; Bonaventura, C.; Bonaventura, J.; Hol, W. G. J. *Proteins* **1994**, *19*, 302−309.

(12) Mahapatra, S.; Young, V. G., Jr.; Tolman, W. B. *Angew. Chem., Int. Ed. Engl.* **1997**, *36*, 130−133.

(13) Mahapatra, S.; Halfen, J. A.; Tolman, W. B. *J. Am. Chem. Soc.* **1996**, *118*, 11575−11586.

(14) (a) Karlin, K. D.; Hayes, J. C.; Gultneh, Y.; Cruse, R. W.; McKown, J. W.; Hutchinson, J. P.; Zubieta, J. *J. Am. Chem. Soc.* **1984**, *106*, 2121−2128. (b) Cruse, R. W.; Kaderli, S.; Karlin, K. D.; Zuberbühler, A. D. *J. Am. Chem. Soc.* **1988**, *110*, 6882−6883. (c) Gelling, O. J.; van Bolhuis, F.; Meetsma, A.; Feringa, B. L. *J. Chem. Soc., Chem. Commun.* **1988**, 552−554. (d) Casella, L.; Gullotti, M.; Pallanza, G.; Rigoni, L. *J. Am. Chem. Soc.* **1988**, *110*, 4221−4224. (e) Menif, R.; Martell, A. E.; Squattrito, P. J.; Clearfield, A. *Inorg. Chem.* **1990**, *29*, 4723−4729. (f) Casella, L.; Gullotti, M.; Bartosek, M.; Pallanza, G.; Laurenti, E. *J. Chem. Soc., Chem. Commun.* **1991**, 1235−1236. (g) Sorrell, T. N.; Vankai, V. A.; Garrity, M. L. *Inorg. Chem.* **1991**, *30*, 207−210. (h) Karlin, K. D.; Nasir, M. S.; Cohen, B. I.; Cruse, R. W.; Kaderli, S.; Zuberbühler, A. D. *J. Am. Chem. Soc.* **1994**, *116*, 1324−1336. (i) Ghosh, D.; Lal, T. K.; Ghosh, S.; Mukherjee, R. *J. Chem. Soc., Chem. Commun.* **1996**, 13−14.

Scheme 2

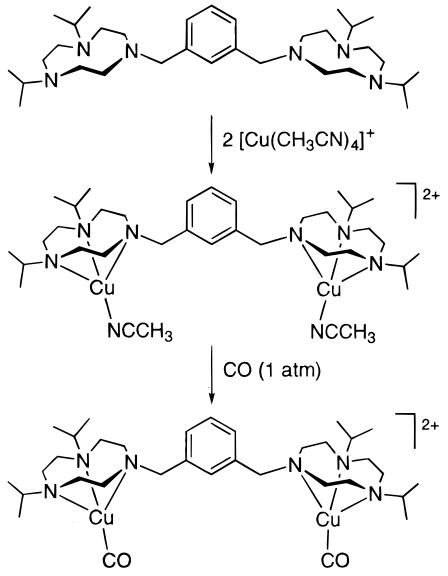

intermediate, postulated to be bent, which due to its disposition underneath the bridging arene ring is able to directly attack the arene π system via an electrophilic pathway.[7c,e,f,14b,h] These results have been interpreted as support for a similar mechanism for phenol hydroxylation by the dicopper active site of tyrosinase.[2,7c,e,f] Here we show through synthetic, structural, and rapid kinetics experiments that the reactivity of the dicopper(I) complex of *m*-XYL^{iPr4} with O_2 is more complicated, with multiple pathways yielding (μ-η^2:η^2-peroxo)dicopper(II) and/or bis(μ-oxo)dicopper(III) cores with different overall complex nuclearities and divergent C−H bond activation reactivities.[15] Overall, these studies have led to a deeper understanding of how ligand topology influences copper−dioxygen chemistry and of the relationship of Cu_n−O_2 complex structure to subsequent oxidative reactivity.

Results

Synthesis and Characterization of Ligands and Complexes. The new ligands *m*-XYL^{iPr4} and *p*-XYL^{iPr4} were prepared by routes analogous to those reported previously for similarly bridged bis(triazacyclononane) systems[16] and were isolated as colorless to pale yellow oils. Derivatives of the *m*-XYL^{iPr4} ligand partially deuterated on the xylyl linker (d_8) or on the isopropyl groups (d_{28}) were targeted for mechanistic experiments (*vide infra*); these were synthesized by coupling α,α′-dibromo-*m*-xylene-d_8 and 1,4-diisopropyl-1,4,7-triazacyclononane (L^{iPr2H})[9b] or α,α′-dibromo-*m*-xylene and L^{iPr2H}-d_{14}, respectively. Copper(I) complexes were prepared by the reaction of [Cu(CH$_3$CN)$_4$]X (X = ClO_4^-, SbF_6^-, $CF_3SO_3^-$) with the appropriate ligands in THF under an inert atmosphere (cf. *m*-XYL^{iPr4} case in Scheme 2). The complexes were isolated as air-sensitive off-white solids and were characterized by elemental analysis, FAB mass spectrometry, and NMR and FTIR spectroscopy. Coordination of a CH$_3$CN ligand to each copper(I) center was confirmed by the observation of a broad singlet at ∼2.3 ppm in ^{1}H NMR spectra (using CD_2Cl_2 as solvent) and a weak ν(C≡N) at ∼2270 cm^{-1} in FTIR spectra. A carbonyl adduct, [(*m*-XYL^{iPr4})Cu$_2$(CO)$_2$](CF$_3$SO$_3$)$_2$, was synthesized by treating the corresponding CH$_3$CN-coordinated complex with 1 atm of CO gas (Scheme 2). A single ν_{CO} was observed in the FTIR spectrum of this compound at 2079 cm^{-1}, intermediate between the values observed for mononuclear carbonyl adducts supported by L^{iPr2Bn} (2069 cm^{-1}) and L^{Bn3} (2084 cm^{-1}).[9b] The small differences between these ν_{CO} bands indicate similar electron-donating characteristics for the mono- and binucleating ligands.

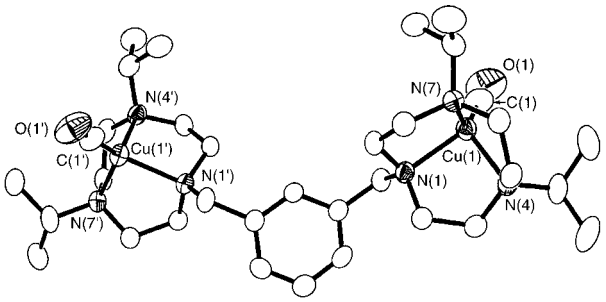

Figure 1. Representation of the cationic portion of the X-ray crystal structure of [(*m*-XYL^{iPr4})Cu$_2$(CO)$_2$](CF$_3$SO$_3$)$_2$·2CH$_2$Cl$_2$ showing all non-hydrogen atoms as 50% ellipsoids (labels for *m*-XYL^{iPr4} ligand atoms omitted for clarity).

Table 1. Selected Bond Lengths (Å) and Angles (deg) for [(*m*-XYL^{iPr4})Cu$_2$(CO)$_2$](CF$_3$SO$_3$)$_2$·2CH$_2$Cl$_2$[a]

Cu(1)−C(1)	1.773(6)	Cu(1′)−C(1′)	1.783(6)
Cu(1)−N(1)	2.103(4)	Cu(1′)−N(1′)	2.105(4)
Cu(1)−N(4)	2.077(4)	Cu(1′)−N(4′)	2.094(4)
Cu(1)−N(7)	2.110(4)	Cu(1′)−N(7′)	2.106(4)
C(1)−O(1)	1.125(7)	C(1′)−O(1′)	1.119(7)
C(1)−Cu(1)−N(4)	126.7(2)	C(1′)−Cu(1′)−N(4′)	128.2(2)
C(1)−Cu(1)−N(1)	123.5(2)	C(1′)−Cu(1′)−N(1′)	125.8(2)
C(1)−Cu(1)−N(7)	132.0(2)	C(1′)−Cu(1′)−N(7′)	128.9(2)
N(4)−Cu(1)−N(1)	86.8(2)	N(4′)−Cu(1′)−N(1′)	85.8(2)
N(4)−Cu(1)−N(7)	87.0(2)	N(4′)−Cu(1′)−N(7′)	87.4(2)
O(1)−C(1)−Cu(1)	177.8(7)	O(1′)−C(1′)−Cu(1′)	179.1(6)

[a] Estimated standard deviations indicated in parentheses.

Confirmation of the topology of *m*-XYL^{iPr4} was obtained from an X-ray crystal structure determination of [(*m*-XYL^{iPr4})-Cu$_2$(CO)$_2$](CF$_3$SO$_3$)$_2$·2CH$_2$Cl$_2$ (Figure 1; selected bond distances and angles listed in Table 1; crystal data shown in Table 2). As in other reported structures for copper(I) complexes of binucleating ligands with flexible linkers,[14a,15a] the ligand adopts an extended conformation with well-separated copper sites [Cu···Cu = 10.061(1) Å]. The metal ion coordination geometries are similar to those observed in other triazacyclononane-supported 4-coordinate copper(I) complexes,[17] and the Cu−CO bonding parameters are typical for this unit.[18]

Oxygenation of the Copper(I) Complexes. (A) Product Identification. Treatment of the solutions of the dicopper(I) complexes of *m*-XYL^{iPr4} or *p*-XYL^{iPr4} with O_2 (1 atm) at −80 °C resulted in the rapid generation of [Cu$_2$(μ-O)$_2$]$^{2+}$ and/or [Cu$_2$-

(15) Competing intra- and intermolecular pathways in the reactions of dicopper(I) complexes of binucleating ligands with dioxygen have been elucidated, although the mechanisms reported differ in many respects from those described here. See: (a) Lee, D.-H.; Wei, N.; Murthy, N. N.; Tyeklár, Z.; Karlin, K. D.; Kaderli, S.; Jung, B.; Zuberhühler, A. D. *J. Am. Chem. Soc.* **1995**, *117*, 12498−12513. (b) Wei, N.; Lee, D.-H.; Murthy, N. N.; Tyeklár, Z.; Karlin, K. D.; Kaderli, S.; Jung, B.; Zuberbühler, A. D. *Inorg. Chem.* **1994**, *33*, 4625−4626.

(16) (a) Brudenell, S. J.; Spiccia, L.; Tiekink, E. R. T. *Inorg. Chem.* **1996**, *35*, 1974−1979. (b) Wieghardt, K.; Tolksdorf, I.; Herrmann, W. *Inorg. Chem.* **1985**, *24*, 1230−1235. (c) Sessler, J. L.; Sibert, J. W.; Lynch, V. *Inorg. Chem.* **1990**, *29*, 4143−4146. (d) Farrugia, L. J.; Lovatt, P. A.; Peacock, R. D. *J. Chem. Soc., Dalton Trans.* **1997**, 911−912.

(17) (a) Chaudhuri, P.; Oder, K. *J. Organomet. Chem.* **1989**, *367*, 249−258. (b) Halfen, J. A.; Mahapatra, S.; Wilkinson, E. C.; Gengenbach, A. J.; Young,V. G., Jr.; Que, L., Jr.; Tolman, W. B. *J. Am. Chem. Soc.* **1996**, *118*, 763−776.

(18) (a) Patch, M. G.; Choi, H.; Chapman, D. R.; Bau, R.; McKee, V.; Reed, C. A. *Inorg. Chem.* **1990**, *29*, 110−119. (b) Karlin, K. D.; Tyeklár, Z.; Farooq, A.; Haka, M. S.; Ghosh, P.; Cruse, R. W.; Gultneh, Y.; Hayes, J. C.; Toscano, P. J.; Zubieta, J. *Inorg. Chem.* **1992**, *31*, 1436−1451.

Table 2. Summary of X-ray Crystallographic Data for $[(m\text{-}XYL^{iPr4})Cu_2(CO)_2](CF_3SO_3)_2\cdot 2CH_2Cl_2$

emp formula	$C_{38}H_{63}Cl_4Cu_2F_6N_6O_8S_2$
fw	1178.94
cryst syst	monoclinic
space group	$P2_1/c$
a (Å)	18.0617(3)
b (Å)	16.6496(4)
c (Å)	18.5594(4)
β (deg)	108.937(1)
V (Å^3)	5279.1(2)
Z	4
D(calc), g cm^{-3}	1.483
temp (K)	173(2)
crystal size (mm)	0.50 × 0.45 × 0.22
diffractometer	Siemens SMART Platform CCD
radiation	Mo Kα (λ 0.710 73 Å)
μ (mm^{-1})	1.159
$2\theta_{max}$ (deg)	50.12
no. of reflns collected	25648
no. of obsd reflns [$I > 2\sigma(I)$]	9190
no. of parameters	603
R1[a]	0.0620
wR2[a]	0.1649
goodness-of-fit	1.028
largest diff peak, hole (e Å^{-3})	0.946, −0.865

[a] $R1 = \Sigma||F_o| - |F_c||/\Sigma|F_o|$; $wR2 = [\Sigma[w(F_o^2 - F_c^2)^2]/\Sigma[w(F_o^2)^2]]^{1/2}$.

$(\mu\text{-}\eta^2\text{:}\eta^2\text{-}O_2)]^{2+}$ cores, identified as such primarily on the basis of their respective UV−vis and/or resonance Raman signatures that were defined in previous studies.[8−12,19] Diagnostic features for the $[Cu_2(\mu\text{-}O)_2]^{2+}$ unit are a pair of absorptions with λ_{max} at ∼320 and ∼435 nm with similar, high extinction coefficients (∼11 000−16 000 M^{-1} cm^{-1} per complex) and a resonance enhanced Cu-O vibration in Raman spectra at ∼600 cm^{-1} that shifts by ∼24 cm^{-1} upon ^{18}O substitution. In contrast, the isomeric $[Cu_2(\mu\text{-}\eta^2\text{:}\eta^2\text{-}O_2)]^{2+}$ core exhibits a different optical absorption pattern with λ_{max} at 360 nm (ϵ ∼20 000 M^{-1} cm^{-1}) and 510 nm (ϵ ∼1000), as well as a peroxide O−O vibration at ∼720−750 cm^{-1} with $\Delta\nu(^{18}O) = 42$ cm^{-1} in Raman spectra.

For the case of the oxygenation of $[(m\text{-}XYL^{iPr4})Cu_2(CH_3CN)_2]^{2+}$, the nature of the product(s) was found to depend on the solvent, the concentration of the starting dicopper(I) complex, and the temperature. High-concentration (≥2.0 mM) CH_2Cl_2 or acetone solutions, as well as THF solutions at any concentration, contain predominantly the bis(μ-oxo)dicopper core, as shown by the characteristic two-band pattern with λ_{max} at 320 and 430 nm in the electronic absorption spectrum (Figure 2(first panel)). Raman spectra ($\lambda_{ex} = 457.9$ nm) of frozen CH_2Cl_2 solutions (∼10 mM) prepared with $^{16}O_2$ or $^{18}O_2$ contain an intense peak at 597 or 573 cm^{-1}, respectively [$\Delta\nu(^{18}O) = 24$ cm^{-1}], and no observable peroxide O−O vibration in the 700−900 cm^{-1} region. In addition, a Cu:O_2 stoichiometry of 2.1-(1):1 was determined by manometric measurement of O_2 uptake. Similar UV−vis and Raman spectral data were obtained for the oxygenated solutions of $[L^{iPr2Bn}Cu(CH_3CN)]^+$ and $[(p\text{-}XYL^{iPr4})Cu_2(CH_3CN)_2]^{2+}$ under all conditions (CH_2Cl_2, acetone, and THF solvents; both low and high concentrations), indicative of bis(μ-oxo) core generation only.[9b]

When the oxygenation of $[(m\text{-}XYL^{iPr4})Cu_2(CH_3CN)_2]^{2+}$ was performed using more dilute (<2.0 mM) CH_2Cl_2 or acetone solutions, mixtures of bis(μ-oxo)- and (peroxo)dicopper species formed. The proportion of the peroxo core, identifiable from a 366 nm absorption signature,[8,11,19] increases when higher temperatures (see discussion of kinetics below) and lower concentration solutions of the dicopper(I) precursor are used (Figure 2). The low optical density of the dilute solutions that contain the peroxo compound as the predominant species (≤0.1 mM) has precluded additional corroboration of the peroxo structure associated with the 366 nm band by resonance Raman spectroscopy.

To explain the concentration dependence of the course of the oxygenation reaction of $[(m\text{-}XYL^{iPr4})Cu_2(CH_3CN)_2]^{2+}$ in CH_2Cl_2 or acetone, we suggest that there is a partitioning between intra- and intermolecular pathways. At low concentration, formation of an intramolecular (peroxo)dicopper complex is favored, whereas at high concentrations, higher nuclearity species with bis(μ-oxo) cores predominate (Scheme 3). As described in more detail below, this model is supported by evidence from kinetics studies, decomposition product analyses, and comparison to the chemistry exhibited by complexes of L^{iPr2Bn} and $p\text{-}XYL^{iPr4}$. A plausible candidate for the higher nuclearity bis(μ-oxo) species is a "dimer-of-dimer" structure, akin to others characterized in studies of iron and manganese complexes of binucleating ligands related to $m\text{-}XYL^{iPr4}$.[20] Consistent with this notion, in the electrospray mass spectrum of the solution obtained upon oxygenation of $[(m\text{-}XYL^{iPr4}\text{-}d_8)Cu_2(CH_3CN)_2](ClO_4)_2$ in CH_2Cl_2 we observed a parent ion envelope at m/z 1691 attibutable to $\{[(m\text{-}XYL^{iPr4}\text{-}d_8)Cu_2(\mu\text{-}O)_2]_2(ClO_4)_3\}^+$. Oligomers of even greater nuclearity than the "dimer-of-dimer" structure are not observable due to mass limitations of our instrumentation, so we cannot rule out their presence. Once formed, the bis(μ-oxo) species supported by $m\text{-}XYL^{iPr4}$, as well as by $p\text{-}XYL^{iPr4}$ or L^{iPr2Bn}, are unaffected by dilution at −70 °C with CH_2Cl_2, acetone, or THF; no conversion to a peroxo species was observed at this low temperature. These results contrast with the behavior of the system supported by L^{iPr3}, which isomerizes between $[Cu_2(\mu\text{-}O)_2]^{2+}$ and $[Cu_2(\mu\text{-}\eta^2\text{:}\eta^2\text{-}O_2)]^{2+}$ cores upon interchanging CH_2Cl_2 and THF solvents.[9a] Importantly, in the current context, the fact that $[(m\text{-}XYL^{iPr4})Cu_2(CH_3CN)_2]^{2+}$ affords upon oxygenation under high-dilution conditions a peroxo species in CH_2Cl_2 or acetone that *cannot* be accessed by dilution of a preformed solution of a bis(μ-oxo) compound (or compounds) further supports our hypothesis of different compositions for the peroxo and bis(μ-oxo) species resulting from divergent intra- and intermolecular pathways, respectively.

(B) Kinetics. Quantitative support for and more detailed insight into the partitioning pathway in Scheme 3 was obtained through variable-temperature stopped-flow kinetics studies of the oxygenation reaction of $[(m\text{-}XYL^{iPr4})Cu_2(CH_3CN)_2](SbF_6)_2$ in acetone. Moreover, analysis of this data in conjunction with (i) data acquired for the like reactions of $[(p\text{-}XYL^{iPr4})Cu_2(CH_3CN)_2]^{2+}$ and $[L^{iPr2Bn}Cu(CH_3CN)]^+$ and (ii) the information obtained previously for compounds supported by L^{iPr3} [9a] and the ethylene-bridged binucleating ligand $i\text{-}Pr_4dtne$[12] has allowed us to obtain a comprehensive description of the oxygenation mechanisms traversed by copper(I) complexes of substituted triazacyclononane ligands.

Specifically, we analyzed the growth of absorbances due to the peroxo and/or bis(μ-oxo) products as a function of time between −82 °C and room temperature according to global, multiple-wavelength methods previously described,[21] including determination of the number of linearly independent absorbing species by factor analysis. A representative plot of observed spectral changes during the oxygenation of $[(m\text{-}XYL^{iPr4})Cu_2]^{2+}$

(19) (a) Solomon, E. I.; Tuczek, F.; Root, D. E.; Brown, C. A. *Chem. Rev.* **1994**, *94*, 827−856. (b) Solomon, E. I.; Baldwin, M. J.; Lowery, M. D. *Chem. Rev.* **1992**, *92*, 521−542.

(20) (a) Sessler, J. L.; Sibert, J. W.; Lynch, V. *Inorg. Chem.* **1990**, *29*, 4143−4146. (b) Gultneh, Y.; Ahvazi, B.; Khan, A. R.; Butcher, R. J.; Tuchagues, J. P. *Inorg. Chem.* **1995**, *34*, 3633−3645.

(21) Karlin, K. D.; Wei, N.; Jung, B.; Kaderli, S.; Niklaus, P.; Zuberbühler, A. D. *J. Am. Chem. Soc.* **1993**, *115*, 9506−9514.

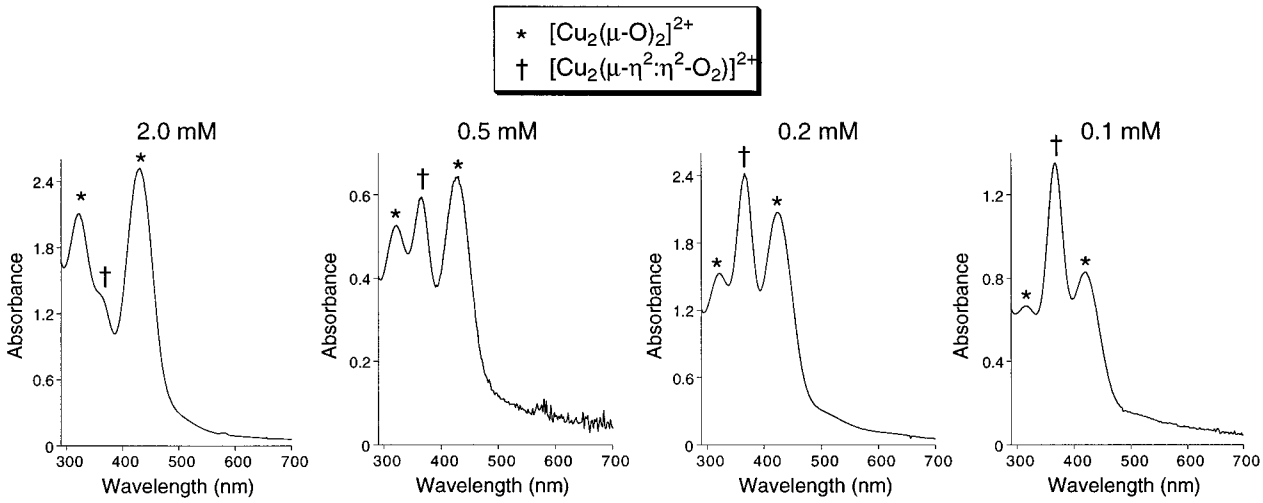

Figure 2. Optical absorption spectra and core assignments of solutions resulting from oxygenation of [(*m*-XYL^{iPr4})$Cu_2(CH_3CN)_2$]$(SbF_6)_2$ in CH_2Cl_2 at the indicated concentrations and −80 °C. Path lengths were 1 mm for 2.0 and 0.5 mM solutions and 1 cm for the 0.2 and 0.1 mM concentrations.

Scheme 3

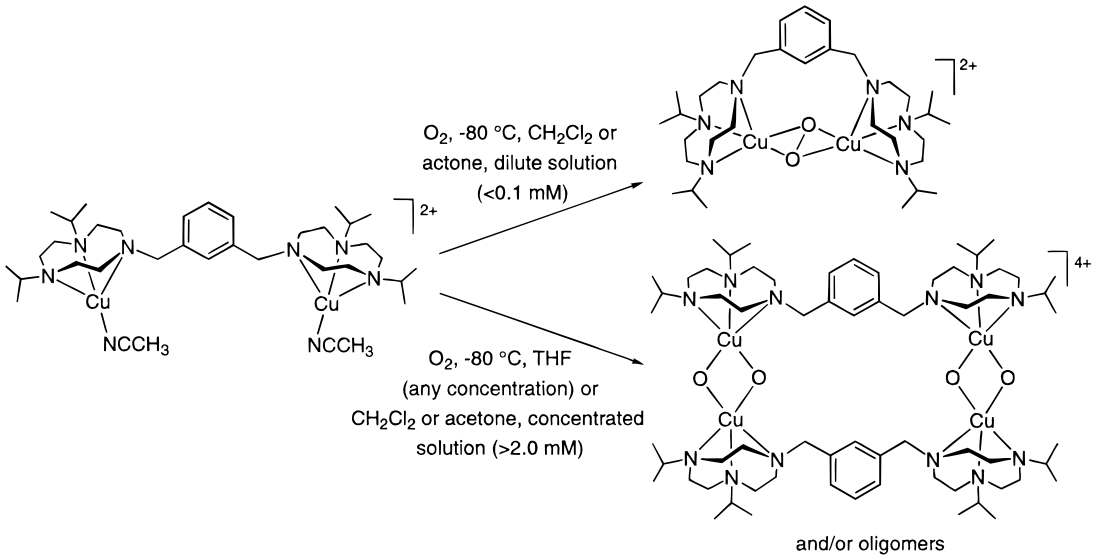

is shown in Figure 3; Eyring plots of the relevant parameters appear in the Supporting Information. The subsequent slower decays of the oxygenated species are described in a later section. A minimum model that explains the kinetic data for the oxygenation reactions for all ligand systems is presented in eqs 2−7 (Charts 1 and 2), where eqs ±2,3 or ±4,5 are conceptually similar reaction steps that are specifically adapted to the complexes of mono- or binucleating ligands, respectively. According to this model, 1:1 Cu:O_2 adduct formation (eq ±2 or ±4) is followed by intermolecular trapping by a second Cu(I) complex (eq 3 and 5) to yield bis(μ-oxo) species in most cases (except L^{iPr3}, which rapidly equilibrates between peroxo and bis(μ-oxo) isomers).[9a] Additional reactions for the complexes of the binucleating ligands had to be considered (Chart 2). These are intramolecular trapping to yield bridged peroxo- or bis(μ-oxo)dicopper compounds (eq 6) and/or further oxygenation of higher nuclearity species to yield "dimer-of-dimer" molecules with two bis(μ-oxo)dicopper units (eq 7, a composite of individual binding and trapping steps). Activation parameters and representative rate constants calculated for selected temperatures are listed in Table 3.

Although initial formation of copper−superoxo species (eq ±2 or ±4) seems to be a necessary first reaction step, at least with the mononuclear starting complexes, we have not obtained direct spectral support for such intermediates by visual inspec-

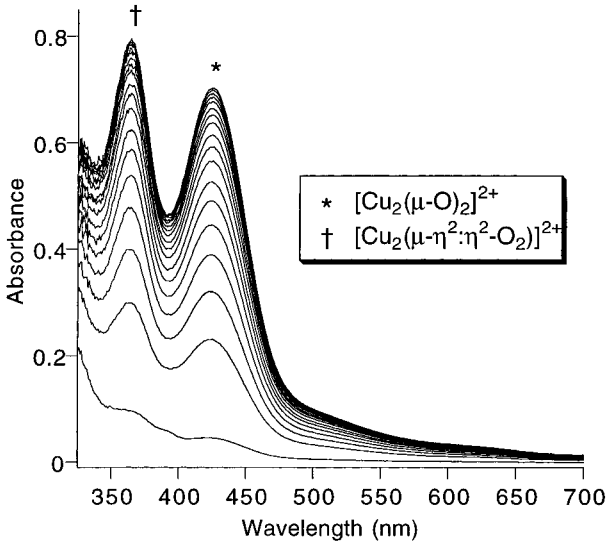

Figure 3. Concomitant formation of (μ-η^2:η^2-peroxo)- (λ_{max} = 364 nm) and bis(μ-oxo)dicopper(II) (λ_{max} = 426 nm) species upon oxygenation of the dicopper(I) complex of *m*-XYL^{iPr4} in acetone. [Complex] = 0.451 mM, [O_2] = 5.813 mM, T = −75.2 °C, and total observation time = 176 s, with 18 out of a total of 125 traces shown for clarity.

Chart 1

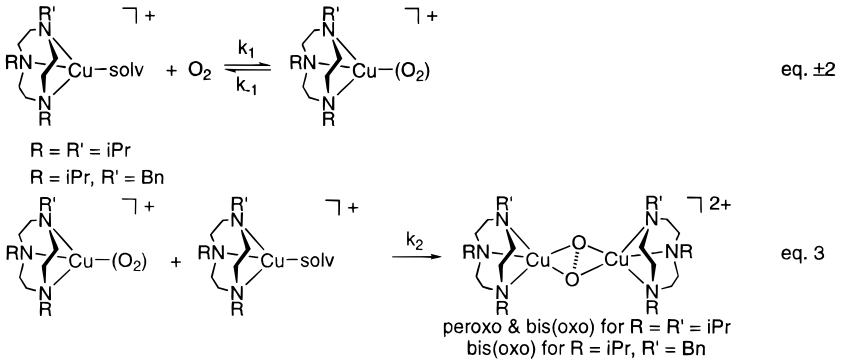

Chart 2

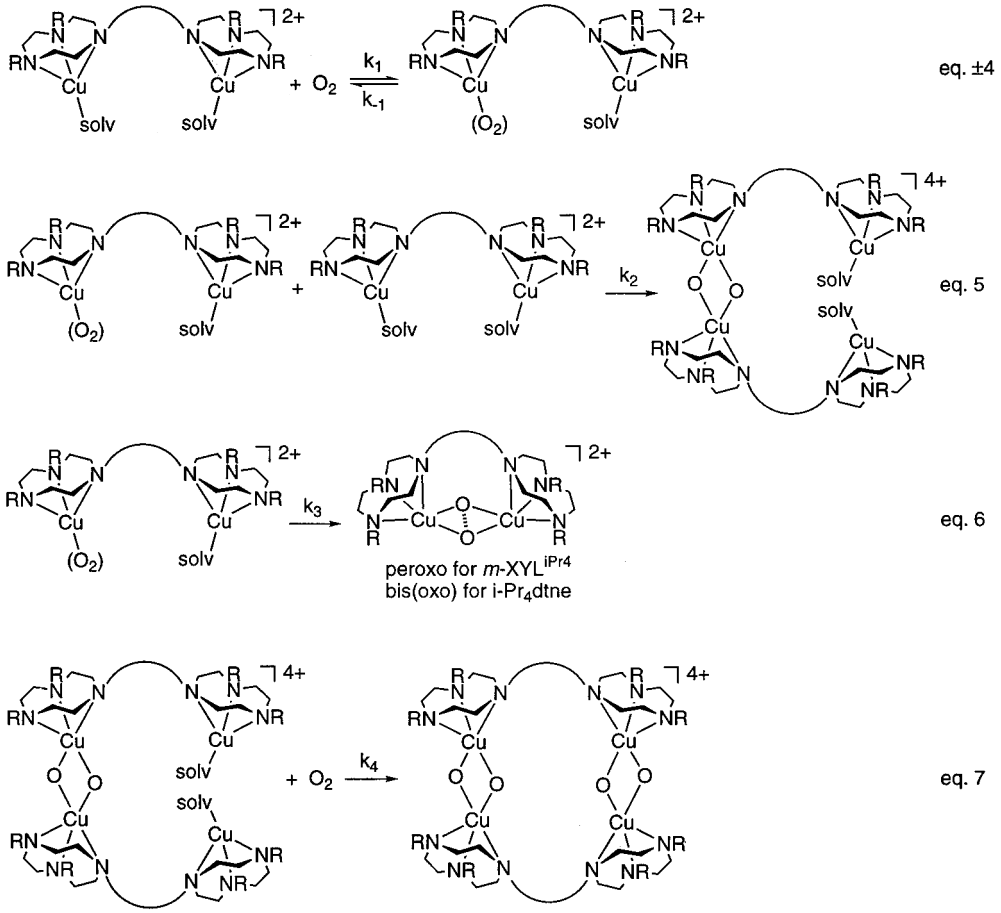

tion or factor analysis of the experimental data for any of the systems so far. Thus, the copper−superoxide species must be treated as steady state species, giving

$$\text{rate} = \frac{k_1[\text{Cu(I)}]^2[\text{O}_2]}{(k_{-1}/k_2) + [\text{Cu(I)}]} \qquad (8)$$

where [Cu(I)] = concentration of copper(I) ions (which for the binucleating ligand cases is 2[complex]). Under certain circumstances, the k_1 step was found to be completely rate-limiting (k_2[Cu(I)] >> k_{-1}, so that rate = k_1[Cu(I)][O_2]), allowing us to directly determine k_1 values and associated activation parameters. This was possible for the complexes of L^{iPr3} and *m*-XYL^{iPr4} at low temperatures (191−223 K and 198−238 K, respectively) and for the complex of *i*-Pr_4dtne in the full temperature range (191−298 K). The characteristics of k_1 are rather similar for the three systems (Table 3); in fact, the rate constants and activation parameters for [(*m*-XYL^{iPr4})Cu_2]$^{2+}$ and [(*i*-Pr_4dtne)Cu_2]$^{2+}$ are identical within experimental error. The activation enthalpy for [L^{iPr3}Cu]$^+$ is also similar, but the overall rate is reduced by an order of magnitude because of a less favorable activation entropy, perhaps due to steric hindrance of solvent exchange by the third isopropyl group.

At given temperatures, kinetic traces for the reactions of [L^{iPr2Bn}Cu]$^+$, [(*m*-XYL^{iPr4})Cu_2]$^{2+}$, and [(*p*-XYL^{iPr4})Cu_2]$^{2+}$ are almost superimposable, showing that there is no dramatic rate enhancement by a chelate effect for the last two complexes. This can be rationalized by assuming that (i) the three complexes that contain identical coordination environments around the individual metal centers have the same intrinsic reactivity toward O_2 and (ii) the formation of the first monocopper adduct (k_1) is essentially rate-limiting. However, for [L^{iPr2Bn}Cu]$^+$ and [(*p*-XYL^{iPr4})Cu_2]$^{2+}$ the back-reaction (k_{-1}) and intermolecular bis(oxo) complex formation (k_2) come into play to some extent,

Table 3. Activation Parameters and Calculated Rate Constants for Oxygenation and Subsequent Decay Reactions of Copper Complexes of the Indicated Ligands (Charts 1−3)

		L^{iPr3}	L^{iPr2Bn}	*m*-XYL^{iPr4}	*p*-XYL^{iPr4}	*i*-Pr_4dtne
	$\Delta H^{\ddagger}$ (kJ mol^{-1})	37.2 ± 0.5	39.4[a]	39.4 ± 0.5	39.4 ± 0.5	39.4 ± 0.1
	$\Delta S^{\ddagger}$ (J K^{-1} mol^{-1})	−62 ± 2	−35.4[a]	−30 ± 2	−30 ± 2	−32.0 ± 0.4
k_1 (M^{-1} s^{-1})	T = 193 K	0.191	*a*	2.46	*a*	1.87
	T = 223 K	5.02	*a*	77.3	*a*	58.8
	T = 273 K	243.2	*a*	4.64×10^3	*a*	3.53×10^3
	$\Delta H^{\ddagger}$ (kJ mol^{-1})	...[c]	22.8 ± 1	...	22.8[b]	...
	$\Delta S^{\ddagger}$ (J K^{-1} mol^{-1})	...	40 ± 5	...	34[b]	...
k_{-1}/k_2 (M)	T = 193 K	...	8.19×10^{-5}	...	*b*	...
	T = 223 K	...	5.54×10^{-4}	...	*b*	...
	T = 273 K	...	5.26×10^{-3}	...	*b*	...
	$\Delta H^{\ddagger}$ (kJ mol^{-1})	...	...	41.7 ± 0.4	24.7 ± 0.7	...
	$\Delta S^{\ddagger}$ (J K^{-1} mol^{-1})	...	...	−28 ± 1	−104 ± 3	...
k_4 (M^{-1} s^{-1})	T = 193 K	...	...	0.71	3.14	...
	T = 223 K	...	...	27.2	28.8	...
	T = 273 K	...	...	2.06×10^3	403.0	...
	$\Delta H^{\ddagger}$ (kJ mol^{-1})	49.1 ± 0.6	56.1 ± 0.9	...	...	58.3 ± 0.4
	$\Delta S^{\ddagger}$ (J K^{-1} mol^{-1})	−79 ± 2	−36 ± 4	...	...	−50 ± 1
k_5 (s^{-1})	T = 193 K	1.59×10^{-5}	3.47×10^{-5}	...	...	1.55×10^{-6}
	T = 223 K	1.13×10^{-3}	4.42×10^{-3}	...	...	2.38×10^{-4}
	T = 273 K	0.177	1.38	...	...	9.23×10^{-2}
	$\Delta H^{\ddagger}$ (kJ mol^{-1})	...	...	31 ± 1	38 ± 2	...
	$\Delta S^{\ddagger}$ (J K^{-1} mol^{-1})	...	...	−151 ± 5	−108 ± 7	...
k_6 (s^{-1})	T = 193 K	...	...	2.07×10^{-4}	6.22×10^{-4}	...
	T = 223 K	...	...	3.22×10^{-3}	1.68×10^{-2}	...
	T = 273 K	...	...	8.42×10^{-2}	0.846	...
	$\Delta H^{\ddagger}$ (kJ mol^{-1})	...	...	...	31.3 ± 0.9	...
	$\Delta S^{\ddagger}$ (J K^{-1} mol^{-1})	...	...	...	−143 ± 3	...
k_7 (s^{-1})	T = 193 K	...	...	...	4.98×10^{-4}	...
	T = 223 K	...	...	...	7.91×10^{-3}	...
	T = 273 K	...	...	...	0.212	...
	$\Delta H^{\ddagger}$ (kJ mol^{-1})	...	...	50.1 ± 0.2		...
	$\Delta S^{\ddagger}$ (J K^{-1} mol^{-1})	...	...	−50.4 ± 0.9		...
k_8 (s^{-1})	T = 193 K	...	...	2.58×10^{-4}	...	...
	T = 223 K	...	...	1.99×10^{-2}	...	...
	T = 273 K			3.44		
	$\Delta H^{\ddagger}$ (kJ mol^{-1})	...	...	76 ± 4	...	...
	$\Delta S^{\ddagger}$ (J K^{-1} mol^{-1})	...	...	−2 ± 12	...	...
k_9 (s^{-1})	T = 193 K	...	...	1.10×10^{-8}	...	...
	T = 223 K	...	...	7.17×10^{-6}	...	...
	T = 273 K	...	...	1.54×10^{-2}	...	...

[a] Value taken from *m*-XYL^{iPr4} case. [b] Value taken from L^{iPr2Bn} case. [c] Not relevant.

necessitating application of eq 8 and, because of the steady state nature of the intermediate 1:1 Cu:O_2 adduct, only allowing elucidation of activation parameters for the ratio k_{-1}/k_2. In principle, k_1 and this ratio could be determined for both systems, but severe correlation of parameters led us to discard this option. Instead, we chose to transfer well-determined parameters between systems, under the assumption that this would be a reasonable approximation because of the close analogies between the individual copper coordination spheres among the various complexes (this was borne out by the characteristics of k_1 described above). Thus, k_1 values from analysis of the data for $[(m\text{-}XYL^{iPr4})Cu_2]^{2+}$ (where consideration of k_{-1} was not needed) were used for analyzing the data for $[(p\text{-}XYL^{iPr4})Cu_2]^{2+}$ and $[L^{iPr2Bn}Cu]^{+}$ (divided by a statistical factor of 2 for the latter). It is worth repeating that the individual metal centers in each of these compounds are alike insofar as they each are coordinated by a triazacyclononane ligand having one benzylic and two isopropyl substituents. The positive enthalpy of activation associated with the composite k_{-1}/k_2 term for the L^{iPr2Bn} complex (23 ± 1 kJ mol^{-1}) is in line with previous observations for other systems;[15a,21] back-reactions (i.e., dissociation of copper−superoxo complexes) are favored relative to binding of a second copper ion at elevated temperatures. These k_{-1}/k_2 values determined for $[L^{iPr2Bn}Cu]^{+}$ (where k_3 and k_4 steps are not involved) then were used for analyzing the data for $[(p\text{-}XYL^{iPr4})Cu_2]^{2+}$ (which are complicated by the additional k_4 step; *vide infra*). As judged by σ(absorbance) values, in no case was the quality of the fitting using this protocol noticeably decreased relative to independent determination of k_1 and k_{-1}/k_2, but the parameter correlation problem was dramatically rectified, yielding a consistent and well-defined picture for the initial stages of the oxygenation reaction.

For both the *m*- and *p*-XYL^{iPr4} systems, additional mechanistic steps that posed difficult kinetics analysis problems had to be taken into account to adequately fit the experimental data. A second oxygenation followed by internal trapping to yield a "dimer-of-dimer" structure was needed for the *p*-XYL^{iPr4} case (k_4 step, eq 7, Chart 2). The large negative activation entropy points to a high degree of reorganization with this highly extended ligand system. Obvious additional steps were tested, such as formation of higher oligomers and partial decay of the monooxygenated, tetracopper intermediate prior to addition of a second O_2 molecule, but strongly correlated parameters and spectra resulted. Since the goodness of fit was already satisfactory without these additional steps, they were not retained in the final analysis. We note in passing that the spectral characteristics of the products of eqs 5 and 7 are essentially identical and are typical for the bis(μ-oxo)dicopper core.

The situation proved to be even more complicated for the most interesting compound of this study, $[(m\text{-XYL}^{iPr4})Cu_2]^{2+}$. As shown in Figure 3 and observed in independent "batch" experiments (*vide supra*), evolution of spectra with characteristics of both peroxo and bis(μ-oxo) species were observed in kinetics experiments, with the product ratios dependent on temperature [peroxo > bis(μ-oxo) as temperature was raised] and the starting complex concentration [bis(μ-oxo) > peroxo as concentration was increased]. In addition, the initial 1:1 Cu:O_2 binding (k_1 step) was rate-limiting throughout and this precluded unique determination of the spectral properties of any of the intermediates shown in Chart 2 or of their corresponding decay products (*vide infra*). As a result, the rate constants for the formation of intermolecular (k_2) and intramolecular (k_3) adducts are almost perfectly correlated (as are the spectra for the respective species). Extensive test calculations showed that the ratio k_3/k_2 could be varied over several orders of magnitude without significantly changing the goodness of fit or the calculated rate constants for subsequent decay (*vide infra*). In the final analysis, a good fit to the experimental data was obtained by setting $k_2 = 16000k_1$ and $k_3 = 2k_2[\text{complex}]_{tot}$ and allowing k_4 to vary. Thus, rather than representing actual kinetic parameters, k_2 and k_3 instead should be regarded as reasonable but arbitrary mechanistic gates that provide for the formation of two independently reacting complexes, the intramolecularly formed peroxo compound (via eq 6) and the initial intermolecular adduct (eq 5). On the other hand, k_4 is a well-defined and real parameter. Extensive testing has verified that its values and the corresponding σ(absorbance) values for the overall fit are independent of the respective values selected for k_2 and k_3, even for k_2/k_3 ratios that vary over 2 orders of magnitude.

The derived activation parameters for the *m*-XYL^{iPr4} k_4 step (Table 3) are quite similar to those for the k_1 step, in contrast to the *p*-XYL^{iPr4} case. This suggests that, for the *m*-XYL^{iPr4} system, 1:1 Cu:O_2 adduct formation again is essentially rate-controlling in the overall k_4 process (eq 7), thus rationalizing the correspondence of the k_1 and k_4 activation parameters, but that subsequent steps contribute in the *p*-XYL^{iPr4} system, making the k_4 parameters truly composite in this case. These differences in kinetic behavior may be due to differences in the disposition of the final Cu(I) ion that collapses to yield the "dimer-of-dimer" product. In other words, one may view the degree of preorganization prior to the final trapping step to be greater in the *meta*-bridged instance than for the more extended *para*-substituted compound, thus making subsequent trapping faster and 1:1 Cu:O_2 adduct formation effectively rate-determining for the former.

Decomposition Reactions of the (Peroxo)- and Bis(μ-oxo)-dicopper Complexes. (A) Product Identification. Upon warming to room temperature, the concentrated (>2.0 mM) orange-brown solutions of the "dimer-of-dimer" and/or oligomeric bis(μ-oxo) species supported by *m*-XYL^{iPr4} turned green. These solutions presumably contain (μ-hydroxo)dicopper(II) compounds like those identified previously for other bis(μ-oxo)-dicopper complex decompositions and possibly akin to that ligated by a *m*-xylyl-bridged bis(1,4,7-triazacyclononane) that was reported recently.[16d] This conclusion is supported by observation of a sharp ν(OH) stretch at ~3640 cm^{-1} in the FTIR spectrum of the solid remaining after removal of solvent. Attempts to isolate pure complexes from the green product solutions have not been successful so far. By treating the green solution with aqueous NH_4OH to remove the copper ions, extracting with CH_2Cl_2, and analyzing the residue remaining after removal of solvent by NMR spectroscopy, we identified two major species in a ratio of 3:2 (~95% mass recovery). These are the unchanged ligand, *m*-XYL^{iPr4}, and the product of N-dealkylation involving loss of an isopropyl group, *m*-XYL^{iPr3H} (Scheme 4). We also detected a minor amount (<5%) of another N-dealkylated product, tentatively identified on the basis of the presence of an ^1H NMR peak at ~10 ppm as the benzaldehyde derived from loss of an *i*-Pr_2TACN fragment. Identical results were obtained from the ligand recovery experiment with the *p*-XYL^{iPr4} system. Analysis of the ligands recovered from the *m*-XYL^{iPr4}-d_{28} system (*i*-Pr groups perdeuterated) revealed a greater proportion of the aldehyde (~15%), (*i*-Pr-d_7)$_2$($CH_2C_6H_4CHO$)TACN, derived from (*i*-Pr-d_7)$_2$TACN scission. The combined results show that N-dealkylation of macrocycle substituents is the major decomposition reaction of the bis(μ-oxo) compounds, with isopropyl group cleavage predominating over attack at the benzylic *m*-xylyl linker position. Entirely analogous regioselectivity was found previously for the reaction of the bis(μ-oxo) complex capped by L^{iPr2Bn}.[13] For *m*-XYL^{iPr4}, the increased amount of benzylic cleavage upon deuteration of the isopropyl groups is consistent with a significant deuterium kinetic isotope effect for the N-dealkylation reaction.[13]

In contrast, when a dilute (<0.1 mM) CH_2Cl_2 solution of $[(m\text{-XYL}^{iPr4})Cu_2(MeCN)_2](SbF_6)_2$ was oxygenated at room temperature, a discrete complex was isolated from the green solution in good yield (55%; Scheme 4). This compound was identified as $[(m\text{-XYL}^{iPr4}\text{-O})Cu_2(\mu\text{-OH})](SbF_6)_2$ on the basis of CHN analysis, FAB mass spectrometry, FTIR and UV−vis spectroscopy, and a preliminary X-ray crystal structure.[22] The FTIR spectrum of the compound contains a sharp ν(OH) at 3632 cm^{-1}. In the UV−vis spectrum, a broad d−d absorption at 680 nm and an intense feature at 380 nm (ϵ 3000 M^{-1} cm^{-1}) were observed, the latter of which we ascribe to a phenolate-to-Cu(II) charge transfer transition by analogy to similar data reported for other (μ-phenoxo)(μ-hydroxo)dicopper(II) compounds.[13a] Although of poor quality due to problems associated with the nature of the crystals we have been able to isolate so far, the X-ray structure confirms the indicated core topology of the complex, the presence of a THF solvent molecule within hydrogen-bonding distance of the bridging hydroxide and, most importantly, the fact that arene hydroxylation rather than N-dealkylation has occurred.[22] We suggest that a $[Cu_2(\mu\text{-}\eta^2\text{:}\eta^2\text{-}O_2)]^{2+}$ species is directly or indirectly responsible for the room-temperature hydroxylation reaction because (i) such a species is generated as the major product in dilute CH_2Cl_2 solution (~0.1 mM) at −80 °C and (ii) stopped-flow kinetics data (*vide supra*) show that the amount of this species increases as the temperature is raised. Further support for this hypothesis was obtained from kinetics experiments (*vide infra*).

(B) Kinetics. As previously described, the decompositions of the peroxo and/or bis(μ-oxo) complexes supported by L^{iPr3}, L^{iPr2Bn}, and *i*-Pr_4dtne are first-order processes that can be described by a single exponential (k_5, eq 9, Chart 3) over a wide range of temperatures.[12,13] For the bis(μ-oxo) cases, oxidative N-dealkylation of an isopropyl group via an intramolecular

(22) In repeated attempts, crystals of the compound were attached to glass fibers and mounted on a Siemens SMART system for data collection at −100 °C. The best results were obtained when a crystal was transferred without warming above ~−50 °C although, even then, it diffracted poorly with 45 s acquisition frames. Some relevant crystal data: monoclinic, space group $P2_1/c$, $a = 11.9887(2)$ Å, $b = 27.0413(2)$ Å, $c = 20.3641(4)$ Å, $\beta = 107.084(1)°$, $V = 6310.5(2)$ Å^3, $Z = 4$; R1 = 0.156 and wR2 = 0.304 for 10 930 independent reflections with $I > 2\sigma(I)$ and 686 parameters. In addition to the dicopper complex and associated counterions, the structure appears to contain two THF and two Et_2O solvent molecules. While we are confident that the topology of the complex as shown in Figure 1 is essentially correct, the poor quality of the structure leads us to hesitate to report or interpret interatomic distance and angle values.

Scheme 4

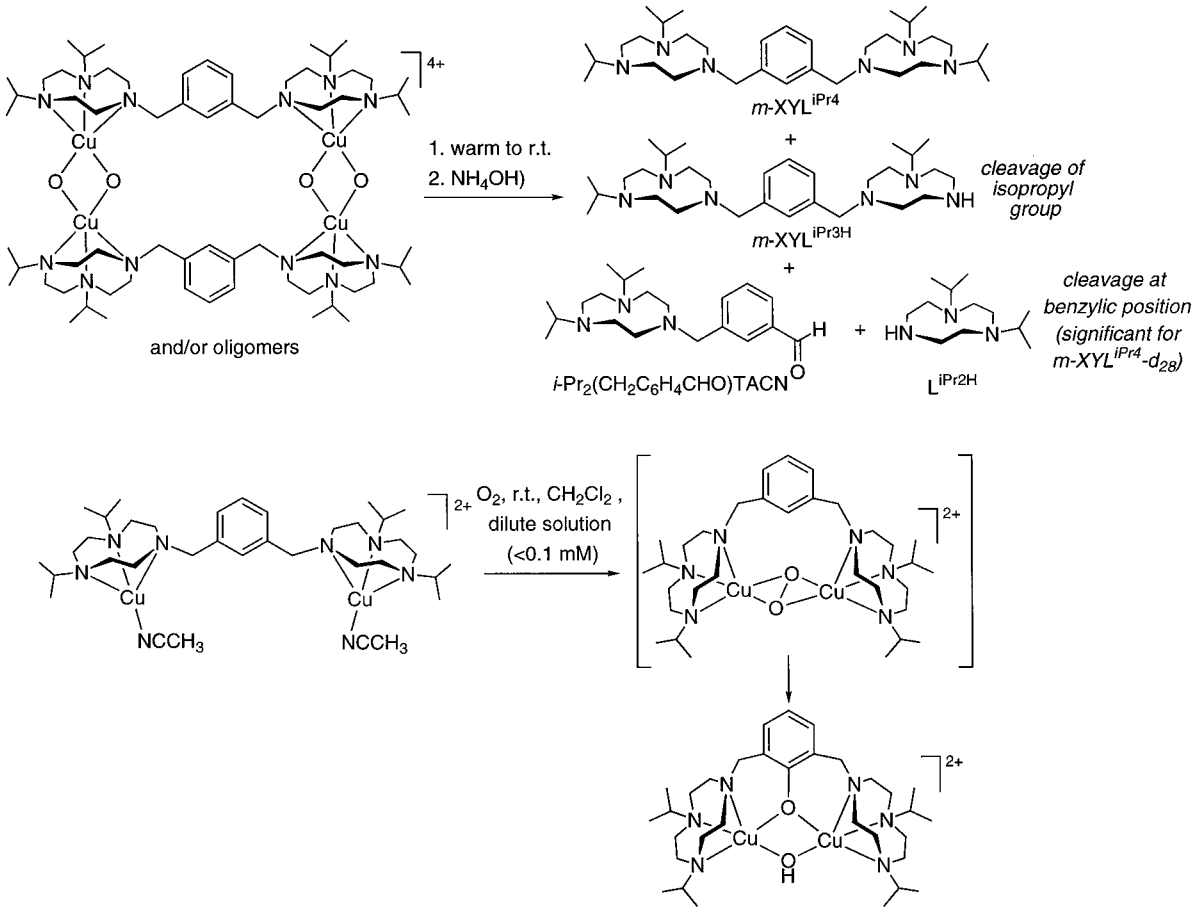

Chart 3

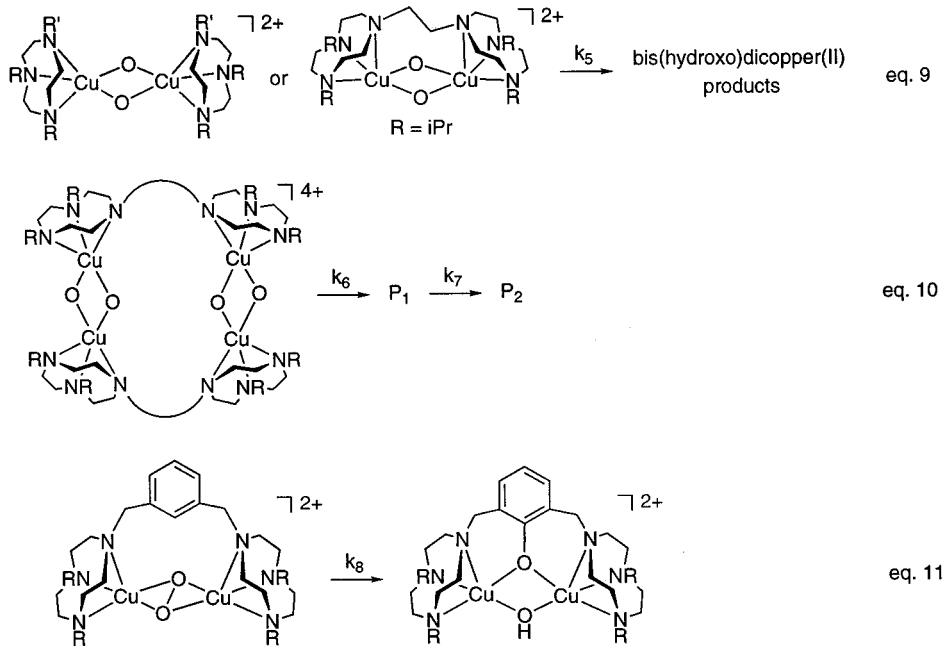

reaction occurs in all cases, with large deuterium KIE's being indicative of methine C−H bond scission during the rate-determining step. For the oxygenated products with *p*- and *m*-XYL^{iPr4}, the decay is more complicated. Numerical analysis of the spectral evolution of the "dimer-of-dimer" bis(μ-oxo) species bound by the *para*-linked ligand was unsatisfactory unless a stepwise process described by the rate constants k_6 and k_7 and products P_1 and P_2, respectively, was invoked (eq 10, Chart 3). These sequential steps are characterized by similar, yet distinct, activation parameters (enthalpies of 30−40 kJ mol^{-1}, strongly negative activation entropies; Table 3). Intermediate P_1 obtained through the first decay (k_6) has spectral properties that are a composite of (i.e., are intermediate between) those of the starting bis[bis(μ-oxo)] complex and the final green [presumably bis(μ-hydroxo)dicopper] products. These combined observations indicate that the two $[Cu_2(\mu\text{-}O)_2]^{2+}$ cores in

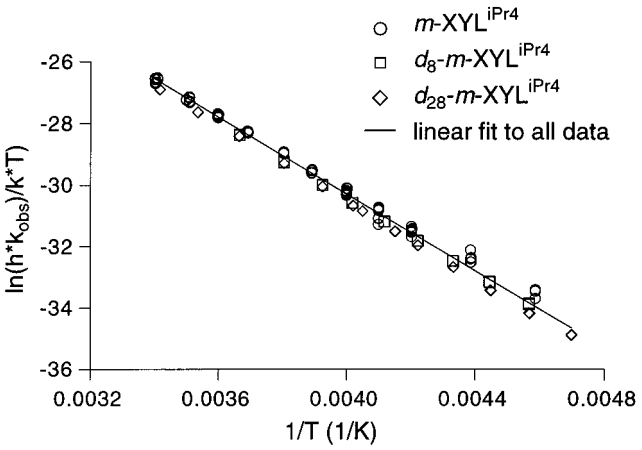

Figure 4. Absence of KIE in peroxo complex decay (k_8): (○) *m*-XYL^{iPr4}, 0.396/0.204/0.102/0.0848 mM; (□) *m*-XYL^{iPr4}-d_8, 0.412 mM; (◇) *m*-XYL^{iPr4}-d_{28}, 0.372 mM; (—) Eyring regression line.

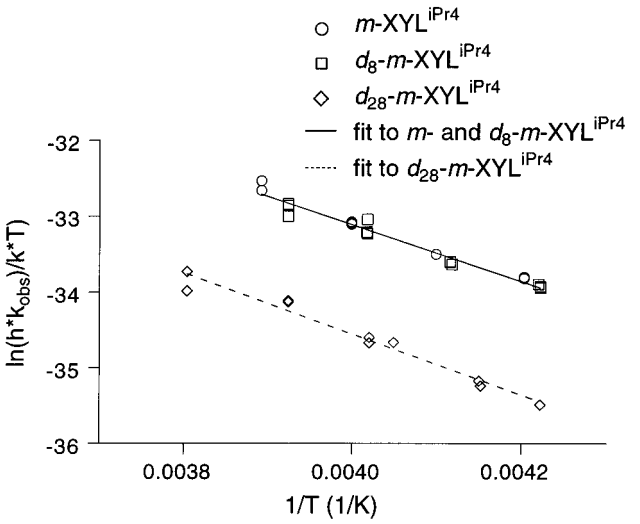

Figure 5. Presence of KIE in bis(oxo) complex decay (k_6): (○) *m*-XYL^{iPr4}, 0.396 mM; (□) *m*-XYL^{iPr4}-d_8, 0.412 mM; (◇) *m*-XYL^{iPr4}-d_{28}, 0.372 mM; (—) Eyring regression line for *m*-XYL^{iPr4} and *m*-XYL^{iPr4}-d_8 cases; (---) Eyring regression line for *m*-XYL^{iPr4}-d_{28} case.

the "dimer-of-dimer" structure react almost independently, producing an intermediate with one bis(μ-oxo)dicopper(III) and one bis(μ-hydroxo)dicopper(II) core.

Further differences were apparent in the decay kinetics for the *m*-XYL^{iPr4} system that is of primary interest in this contribution. Significantly, different kinetic behaviors were found for the decay monitored at 365 nm (peroxo species, k_8, eq 11, Chart 3) and at 420 nm [bis(μ-oxo), k_6 and k_9]. The activation parameters for k_8 (Table 3) closely agree with those determined previously for the arene hydroxylation reaction of the peroxo complex supported by a *m*-xylyl-bridged bis(2-pyridylethyl)amine chelate; $\Delta H^{\ddagger}$ values are identical within experimental error, 50.1 ± 0.2 (this work) and 50 ± 1[14h] kJ mol^{-1}, respectively, and the $\Delta S^{\ddagger}$ values are both negative, −50 (this work) and −35 J K^{-1}mol^{-1}.[14h] We thus interpret k_8 as the rate constant for arene hydroxylation by the intramolecular peroxo adduct supported by *m*-XYL^{iPr4}. The decay primarily associated with the 420 nm feature is described by k_6, which has characteristics similar to those of the analogous step in the decay of the tetranuclear bis[bis(μ-oxo)] complex supported by *p*-XYL^{iPr4}. In principle, one would expect a two-step decay for the *meta*-bridged "dimer-of-dimer" bis(μ-oxo) species like that described above for the *para*-substituted system, but this was not detected, perhaps due in part to the obscuring effect of the additional peroxo species. Instead, another secondary decay at high temperatures (k_9) was observed with fundamentally different activation parameters and associated spectral changes. We have no mechanistic interpretation for k_9 at present, but an analogous reaction is also detectable with L^{iPr2Bn} as the supporting ligand for $T > 0$ °C.

Further insights into the nature of the *m*-XYL^{iPr4} system decay were obtained through the examination of the kinetics of the reactions of selectively deuterated derivatives. These are *m*-XYL^{iPr4}-d_8, in which only the *m*-xylyl portion is isotopically substituted, and *m*-XYL^{iPr4}-d_{28}, which is only labeled at the isopropyl groups. As anticipated, in no instance did ligand deuteration influence the oxygen-binding kinetics. More importantly, the values of k_8 (peroxo decay) were identical at all temperatures for the parent case and both deuterated derivatives (Figure 4). For k_6 [bis(μ-oxo) decay], however, a significant KIE ($k_H/k_D = 4.6$ at −40 °C) was observed for the d_{28}-labeled-isopropyl derivative but not for the d_8-labeled-xylyl case (Figure 5). These results nicely corroborate assignments of intermediates and processes based on product analysis and primary kinetics. Thus, k_8 pertains to arene hydroxylation by the intramolecular μ-η^2:η^2-peroxo complex, for which no KIE is expected on the basis of previous studies on analogous *m*-xylyl-bridged systems.[14b,23] No attack of benzylic or isopropyl substituent C−H bonds is involved. The k_6 step describes N-dealkylation by the bis(μ-oxo) core in which rate-controlling C−H bond scission occurs primarily at a substituent isopropyl group, thus explaining the observation of a significant KIE when isopropyl, but not xylyl, groups are deuterated. However, the observed KIE is smaller than those described previously for N-dealkylations by other bis(μ-oxo) species supported by L^{Bn3}, L^{iPr3}, or *i*-Pr$_4$dtne.[12,13] The reason for this is not clear at present. Possible explanations include a contribution from benzylic C−H bond cleavage in the d_{28} system (this is supported by our observation of increased amounts of benzylic dealkylation products in ligand recovery experiments; *vide supra*) and/or undefined influences of specific geometrical features of the "dimer-of-dimer" structure on the transition state geometry. Slow interconversion between intra- and intermolecular adducts might also affect the observed KIE and cannot be ruled out at the higher temperatures at which the decay kinetics were measured.

Discussion

New insights into the factors responsible for observation of either the (μ-η^2:η^2-peroxo)- or bis(μ-oxo)dicopper core and into their respective C−H bond activation reactivities may be gleaned from a comparison of the previously described oxygenation chemistry of copper(I) complexes supported by the ligands L^{iPr3}, L^{Bn3}, L^{iPr2Bn},[9] and *i*-Pr$_4$dtne[12] with that described herein for *p*-XYL^{iPr4} and *m*-XYL^{iPr4}. In general, the initial 1:1 Cu:O$_2$ reaction to yield a transient, as yet unobserved, adduct [presumably a Cu(II)−superoxo species] is to a large extent rate-controlling for all of these triazacyclononane-based ligand systems, with variations in the nature of the final oxygenated products being the result of differences in the subsequent, generally faster pathway(s). While ligand composition appears to have little effect on the initial 1:1 Cu:O$_2$ adduct formation, the following steps are dramatically influenced. From a comparison of a series of *N*,*N*′,*N*″-trisubstituted mononucleating ligands,[8,9,24] it has become evident that the bis(μ-oxo)dicopper core is the favored final product unless there is branching at the carbon α to each N donor atom (as in, for example, L^{iPr3},

(23) Nasir, M. S.; Cohen, B. I.; Karlin, K. D. *J. Am. Chem. Soc.* **1992**, *114*, 2482−2494.
(24) Schaller, C.; Berreau, L. M.; Halfen, J. A.; Mahapatra, S.; Tolman, W. B. Unpublished results.

but not L^{iPr2Bn}). We hypothesize that such branching provides sufficient steric hindrance to inhibit collapse to the contracted bis(μ-oxo)dicopper unit (Cu···Cu = 2.8 Å) and thus to enforce generation under certain conditions of the more extended (μ-η^2:η^2-peroxo)dicopper structure (Cu···Cu = 3.6 Å). This branching is not present at every α-carbon in *i*-Pr_4dtne, and the short ethyl linker in this bis(macrocyclic) ligand supports rapid intramolecular closure of the initial 1:1 Cu:O_2 complex to a bis(μ-oxo)dicopper unit. In this entropically favored reaction, the short linker further disfavors the longer intercopper separation intrinsic to the (μ-η^2:η^2-peroxo)dicopper framework.

For the *p*-XYL^{iPr4} ligand system examined herein, the long and relatively stiff tether between the macrocyclic chelates favors inter- rather than intramolecular reaction of the first 1:1 Cu:O_2 species to ultimately afford higher nuclearity species with bis(μ-oxo)dicopper components. That the μ-η^2:η^2-peroxo isomer is not observed is consistent with the 1-benzyl-4,7-diisopropyl substitution pattern of each macrocycle; each triazacyclononyl−copper unit in $[p\text{-}XYL^{iPr4}Cu_2]^{2+}$ reacts essentially independently like monomeric $[L^{iPr2Bn}Cu]^+$ to yield bis(μ-oxo)dicopper cores. For the *m*-XYL^{iPr4} ligand, we see interesting chemistry intermediate between the respective extremes defined for *i*-Pr_4dtne and *p*-XYL^{iPr4}. Temperature- and concentration-dependent partitioning of the 1:1 Cu:O_2 adduct between intra- and intermolecular pathways occurs, which in the latter case yields higher nuclearity species with bis(μ-oxo) units just like *p*-XYL^{iPr4}. While subtle differences in the steps involved in "dimer-of-dimer" formation are evident from the stopped-flow kinetics studies (e.g., the k_4 step, eq 7, Chart 2) that appear to reflect the divergent overall structures of intermediates supported by the two isomeric *p*- and *m*-xylyl-bridged ligands, it is the local resemblance of each monocopper component to $[L^{iPr2Bn}Cu]^+$ that gives rise to bis(μ-oxo)dicopper formation in the intermolecular reactions of each. In the intramolecular reaction of *m*-XYL^{iPr4}, however, the linker that is more extended than that in *i*-Pr_4dtne inhibits collapse to the contracted core and instead favors a μ-η^2:η^2-peroxo species.

The course of the decomposition reactions of the various oxygenated products directly reflects their structures, as the site of oxidative attack on the ligand in each case is determined by the relative disposition of the ligand and peroxo or bis(μ-oxo) components. N-dealkylation of isopropyl substituents is the predominant pathway for all of the bis(μ-oxo) compounds, including those with additional benzylic substituents (L^{iPr2Bn} and *p*- and *m*-XYL^{iPr4}). This regioselectivity is somewhat surprising in view of the expectation of enhanced intrinsic reactivity of the benzylic C−H bond and points toward a geometric rationale. Previously reported X-ray crystal structures of the bis(μ-oxo) complexes supported by L^{Bn3} and *i*-Pr_4dtne show short intramolecular contacts between the hydrogen atoms on the α-carbons of equatorially disposed ligand substituents and the electrophilic, bridging oxo groups, leading us to suggest that the transition state for the rate-determining attack of the oxo unit at these C−H bonds evolves from this ground state interaction. We speculate that the preference for isopropyl over benzyl N-dealkylation may arise from a predilection for positioning of the isopropyl-substituted N donors in the equatorial coordination position, placing the isopropyl methine C−H bonds, rather than the axially disposed benzylic congeners, near the reactive oxo group. This structural argument seems applicable to the cases involving the XYL^{iPr4} ligands (based on ball-and-stick models, for example), although support in the form of direct information on the topology of these bis(μ-oxo) species remains elusive. The ground state predisposition for isopropyl attack is offset upon selective deuteration of these groups in *m*-XYL^{iPr4}-d_{28} by the significant dimunition of the rate of C−D bond scission from an intrinsically large deuterium KIE. However, while a KIE value similar to those measured for L^{Bn3} and L^{iPr3} (k_H/k_D at −40 °C = 40 and 26, respectively) would be expected, the observed value is 4.6. Although other explanations may be applied (*vide supra*), this smaller value for *m*-XYL^{iPr4}-d_{28} may be traced, at least in part, to the occurrence of competitive benzylic C−H bond cleavage, which cannot interfere for the cases of L^{Bn3} or L^{iPr3} because all identical substituents are similarly labeled. Inherent in this model is the need for equatorial and axial N donors to rapidly exchange, perhaps via a "turnstile" process, so that the benzylic C−H bonds may present themselves to the oxo bridge for attack. In support of a "turnstile" exchange mechanism, theory has shown it to have a low barrier in a bis(μ-oxo)dicopper model compound with terminal NH_3 ligands.[9b] Moreover, it explains the signal averaging seen in ^{1}H NMR spectra of the bis(μ-oxo)dicopper complex capped by L^{Bn3}. Exchange of axial and equatorial donors cannot be accommodated in the intramolecular bis(μ-oxo) compound ligated by *i*-Pr_4dtne, consistent with the fully expressed KIE at −40 °C of 40 (isopropyls but not ethyl linker labeled) and the complete N-dealkylation regioselectivity observed (removal of a single isopropyl group only).[12]

Consistent with its intramolecular formulation, in the μ-η^2:η^2-peroxo complex of *m*-XYL^{iPr4} the peroxide attacks the bridging arene ring of *m*-XYL^{iPr4} to yield hydroxylated product. This type of conversion is now well-precedented, albeit with a somewhat limited set of supporting ligands.[14] The arguments put forth by Karlin and co-workers to rationalize the hydroxylation reactions of their arene-bridged dinucleating ligand systems are equally applicable here,[7e−g,14h] particularly in view of our observation of similar activation parameters and a lack of a KIE upon deuteration of the arene ring. Thus, by analogy, we suggest that the peroxo unit resides in close proximity to the bridging arene π system, predisposing attack at the arene in preference to the isopropyl substituents. The available experimental data are equally compatible with synchronous or consecutive O−O bond breaking and attack on the arene; in other words, either the observed peroxo unit or a derived, heretofore unobserved, bis(μ-oxo) species may be the actual reactant. Both ball-and-stick models and preliminary molecular mechanics calculations[25] point to direct interaction of an oxygen atom with the C-2 arene carbon, rather than primary hydrogen abstraction.

Concluding Remarks

The multistep copper−dioxygen chemistry we have observed has revealed decisive control by ancillary ligand structural elements over the type of products formed [peroxo vs bis(μ-oxo), intra- vs intermolecular], the rates of elementary oxygenation reaction steps, and the course of subsequent C−H bond activation pathways (N-dealkylation vs arene hydroxylation). Similar influences have been uncovered in separate studies incorporating mixed pyridyl−amine ligands, where reaction pathways complementary to those described herein were identified.[7c,e−g,15] The ligand structural effects generally appear to be steric in origin, leading us to favor the notion that this type of steric control over oxygenation and C−H bond activation mechanisms also may be important in metalloenzyme processes.

(25) Molecular Mechanics calculations were performed on a Silicon Graphics IRIS Indigo R 4000 computer using Cerius^2 (Molecular Simulations Inc., Version 1.6) software based on the Universal FF force field module. Independent of several restrictions, a closest approach of about 2.70 Å between one of the bridging oxygen atoms and the C-2 arene carbon was obtained.

Further comprehensive spectroscopic, structural, and mechanistic studies of synthetic systems will allow the detailed nature of copper−dioxygen reaction pathways and intermediates in synthetic systems to be unraveled and will provide precedent for such hypotheses of related structures and mechanisms within the biological (copper protein) milieu.

Experimental Section

General Procedures. All reagents and solvents were obtained from commercial sources and used as received unless noted otherwise. Solvents were dried according to published procedures[26] and distilled under N_2 immediately prior to use. Dioxygen gas was dried by passing through two short columns of supported P_4O_{10} and Drierite. Labeled dioxygen ($^{18}O_2$, 99%) was obtained from Cambridge Isotopes, Inc., and used without further purification. All air-sensitive reactions were performed either in a Vacuum Atmospheres inert-atmosphere glovebox under a N_2 atmosphere or by using standard Schlenk and vacuum line techniques. The salts $[Cu(CH_3CN)_4]X$ ($X = ClO_4^-$, SbF_6^-, $CF_3SO_3^-$) were prepared as described in the literature.[27] The precursors for the dinucleating ligands, 1,4-bis(*p*-tolylsulfonyl)-1,4,7-triazacyclononane (L^{Ts2H})[20a] and 1,4-diisopropyl-1,4,7-triazacyclononane (L^{iPr2H})[9b] were synthesized using published procedures. 2-Bromopropane-d_7 [$(CD_3)_3$-CDBr, 98%] was purchased from Aldrich and used as received, whereas other deuterium-labeled precursors, α,α′-dibromo-*m*-xylene-d_8[28] and 1,4-di(isopropyl-d_7)-1,4,7-triazacyclononane (L^{iPr2H}-d_{14})[9b,13] were synthesized by reported procedures. Deuterium incorporation was determined by integration of the residual proton signals in the ^1H NMR spectra of the compounds. Elemental analyses were performed by Atlantic Microlabs, Norcross, GA. Physical methods used for compound characterization are described elsewhere.[9b]

Stopped-Flow Experiments. Rapid kinetics were followed using an SF-21 variable-temperature stopped-flow unit (Hitech) combined with a TIDAS-16 HQ/UV−vis 512/16B diode array spectrometer (J & M; 507 diodes, 300−720 nm, 1.3 ms minimum sampling time). Data acquisition (up to 256 complete spectra; up to four different time bases) was performed by using the Kinspec program (J & M). For numerical analysis, all data were pretreated by factor analysis and concentration profiles based on various kinetic models were calculated by numerical integration using either Kinfit[21,29] or Specfit (Spectrum Software). Acetone (Uvasol, Merck) was used without further purification. Thermal expansion of the solvent was taken into account using ρ (g/mL) $= -1.1248 \times 10^{-3}\ T$ (K) $+ 1.1218$ for the solvent density as function of temperature. For further details, see ref 21. The temperature was varied between 198 and 294 K, and the initial O_2 concentration was 5.106 mM for all systems studied.

For $[L^{iPr2Bn}Cu]^+$, three series of experiments were performed with 0.522, 0.384, and 0.163 mM complex concentrations (room temperature), respectively. Data for a total of 131 individual runs with data collection times between 2 and 521 s were obtained. Of these, 39 data sets were used for the final analysis based on the complete model (formation and decay of bis(μ-oxo) complex), while the others (short collection times) served for additional validation of the initial stages of the reaction.

$[(m\text{-}XYL^{iPr4})Cu_2]^{2+}$ was studied by using four series (0.396, 0.204, 0.102, 0.0848 mM) with undeuterated ligand and two series with substituted $[(m\text{-}XYL^{iPr4}\text{-}d_8)Cu_2]^{2+}$ (0.412 mM) and $[(m\text{-}XYL^{iPr4}\text{-}d_{28})Cu_2]^{2+}$ (0.372 mM), respectively. Data for a total of 155 (unsubstituted), 30 (d_8), and 26 (d_{28}) individual runs were included in the final analysis. Collection times were varied between 0.3 and 2170 s.

$[(p\text{-}XYL^{iPr4})Cu_2]^{2+}$ was studied by using three series (0.333, 0.154, 0.0753 mM). Data for a total of 143 individual runs were taken and analyzed, of which 41 data sets were used to obtain the final parameters. Collection times were varied between 1.4 and 586 s.

Safety Note. ***Caution!*** *Perchlorate salts of metal complexes with organic ligands are potentially explosive. Only small amounts of material should be prepared, and these should be handled with great care.*

α,α′-Bis[4,7-bis(*p*-tolylsulfonyl)-1,4,7-triazacyclononan-1-yl]-*m*-xylene (*m*-XYL^{Ts4}). 1,4-Bis(*p*-tolylsulfonyl)-1,4,7-triazacyclononane (2.0 g, 4.5 mmol) and α,α′-dibromo-*m*-xylene (0.58 g, 2.2 mmol) were dissolved in CH_3CN (15 mL). Solid Na_2CO_3 (∼2.0 g) was added to the solution, and the resultant mixture was heated at reflux under a N_2 atmosphere for 1 day. After cooling to room temperature, the mixture was filtered, and the filtrate was then washed with $CHCl_3$ and dried with anhydrous $MgSO_4$. Removal of solvent under reduced pressure afforded 2.15 g (96%) of an off-white solid. ^1H NMR ($CDCl_3$, 300 MHz): δ 7.63 (d, $J = 7.4$ Hz, 8H), 7.40−7.31 (m, 12H), 3.72 (s, 4H), 3.45 (s, 8H), 3.11 (s, br, 8H), 2.95 (s, br, 8H), 2.42 (s, 12H) ppm. $^{13}C\{^1H\}$ NMR ($CDCl_3$, 75 MHz): δ 142.8, 138.7, 134.9, 129.2, 129.1, 127.4, 127.3, 126.6, 60.4, 54.1, 51.9, 50.9, 20.9 ppm. Anal. Calcd for $C_{48}H_{60}N_6O_{12}S_4$: C, 55.37; H, 5.81; N, 8.08. Found: C, 55.72; H, 6.10; N, 8.37.

α,α′-Bis(1,4,7-triazacyclononan-1-yl)-*m*-xylene (*m*-XYL^{H4}). The precursor *m*-XYL^{Ts4} (3.2 g, 3.3 mmol) was dissolved in concentrated H_2SO_4 (10 mL), and solution was heated at 100 °C under a N_2 atmosphere for 48 h. The resulting deep brown solution was cooled in an ice bath and brought to pH >12 by the *cautious* addition of 15 N NaOH. It was then extracted with $CHCl_3$ (5 × 100 mL), and the organic layers were combined and dried over anhydrous $MgSO_4$. Following the removal of solvent, the product was obtained as a colorless oil (0.90 g, 76%). ^1H NMR ($CDCl_3$, 500 MHz): δ 7.32−7.18 (m, 4H), 3.68 (s, 4H), 2.75 (s, 8H), 2.64−2.60 (m, 16H), 2.30 (s, br, 4H) ppm. $^{13}C\{^1H\}$ NMR ($CDCl_3$, 125 MHz): δ 139.8, 129.6, 128.2, 127.7, 61.6, 52.8, 46.7, 46.5 ppm. Anal. Calcd for $C_{20}H_{36}N_6$: C, 62.09; H, 9.05; N, 11.43. Found: C, 61.95; H, 9.15; N, 11.45.

α,α′-Bis(4,7-diisopropyl-1,4,7-triazacyclononan-1-yl)-*m*-xylene (*m*-XYL^{iPr4}). This compound was synthesized by two different routes.

Method A. To a solution of *m*-XYL^{H4} (0.90 g, 2.50 mmol) in toluene (10 mL) was added isopropyl bromide (1.9 g, 15.08 mmol). The solution was refluxed for 2 h, at which time solid KOH (∼2.0 g) was added; the mixture was then refluxed overnight. After the resulting mixture was cooled to room temperature, the precipitated KCl and unreacted KOH were removed by filtration, the filtrates were washed with $CHCl_3$, and the combined filtrates were dried with anhydrous $MgSO_4$. Removal of solvent under reduced pressure afforded the desired ligand as a light yellow oil (0.95 g, 72%).

Method B. A toluene solution (10 mL) of L^{iPr2H} (1.20 g, 5.68 mmol) and α,α′-dibromo-*m*-xylene (0.75 g, 2.84 mmol) was refluxed for 2 h, at which time solid KOH (∼ 2.0 g) was added; the mixture was then refluxed overnight under a N_2 atmosphere. After cooling to room temperature, the mixture was filtered through a Celite pad, and solvent was then removed to yield a thick, light yellow oil. If required, the ligand can be purified by isolating the protonated version obtained upon treatment with $NaClO_4$ in MeOH, followed by regenerating the free base with KOH in toluene, according to the method described previously for the purification of 1,4,7-triisopropyl-1,4,7-triazacyclononane.[30] Yield: 1.34 g (89%). ^1H NMR ($CDCl_3$, 300 MHz): δ 7.15−7.33 (m, 4H), 3.65 (s, 4H), 2.96−2.86 (m, 12H), 2.61 (s, 16H), 0.95 (d, $J = 6.6$ Hz, 24H) ppm. $^{13}C\{^1H\}$ NMR ($CDCl_3$, 75 MHz): δ 140.1, 129.7, 127.4, 125.3, 62.1, 55.0, 54.8, 52.3, 52.1, 18.5 ppm. LREIMS, *m/z* (relative intensity, assignment): 528.5 (10, $[M - H]^+$), 430.4 (100). Anal. Calcd for $C_{32}H_{60}N_6$: C, 72.66; H, 11.44; N, 15.90. Found: C, 72.43; H, 11.22; N, 15.04.

The isotopomer *m*-XYL^{iPr4}-d_8 (deuterated at the xylyl portion) was synthesized similarly to method B except that α,α′-dibromo-*m*-xylene-d_8 was used. Deuterium content: 99%. ^1H NMR ($CDCl_3$, 500 MHz): δ 2.94−2.87 (m, 12H), 2.61 (s, 16H), 0.95 (d, $J = 6.6$ Hz, 24H) ppm. LRCIMS, *m/z* (relative intensity, assignment): 537.6 (100, M^+). The isotopomer *m*-XYL^{iPr4}-d_{28} (deuterated isopropyl groups) was synthesized similarly by reacting α,α′-dibromo-*m*-xylene (0.12 g, 0.47 mmol) with L^{iPr2H}-d_{14} (0.20 g, 0.94 mmol). Deuterium content: 98%. ^1H NMR ($CDCl_3$, 500 MHz): δ 7.34 (s, 1H), 7.22 (s, br, 3H), 3.65 (s, 4H),

(26) Perrin, D. D.; Armarego, W. L. F. *Purification of Laboratory Chemicals*; Pergamon Press: New York, 1988.
(27) Kubas, G. J. *Inorg. Synth.* **1979**, *19*, 90−92; **1990**, *28*, 68−70.
(28) Cruse, R. W.; Kaderli, S.; Meyer, C. J.; Zuberbühler, A. D.; Karlin, K. D. *J. Am. Chem. Soc.* **1988**, *110*, 5020−5024.
(29) Jung, B. Ph.D. Thesis, University of Basel, Switzerland, 1994.
(30) Haselhorst, G.; Stoetzel, S.; Strossburger, A.; Walz, W.; Wieghardt, K.; Nuber, B. *J. Chem. Soc., Dalton Trans.* **1993**, 83−90.

2.89−2.86 (m, 8H), 2.62−2.59 (m, 16H) ppm. LRCIMS *m/z* (relative intensity, assignment): 557.4 (100, M^+).

α,α′-Bis(4,7-diisopropyl-1,4,7-triazacyclononan-1-yl)-*p*-xylene (*p*-XYL^{iPr4}). Using the same procedure (method B) as described for the synthesis of *m*-XYL^{iPr4}, α,α′-dibromo-*p*-xylene (0.12 g, 0.47 mmol) and L^{iPr2H} (0.20 g, 0.94 mmol) were reacted to yield 0.22 g of *p*-XYL^{iPr4} as a thick yellow oil (88%). ^{1}H NMR ($CDCl_3$, 300 MHz): δ 7.36 (d, J = 1.0 Hz, 4H), 7.26 (d, J = 1.0 Hz, 4H), 3.63 (s, 4H), 2.95−2.82 (m, 12H), 2.61 (s, 16H), 0.94 (d, J = 6.6 Hz, 24H) ppm. ^{13}C{^{1}H} NMR ($CDCl_3$, 75 MHz): δ 138.9, 128.7, 62.1, 55.3, 54.8, 52.7, 52.4, 18.5 ppm. LREIMS, *m/z* (relative intensity, assignment): 528.5 (10, $[M - H]^+$), 430.4. Anal. Calcd for $C_{32}H_{60}N_6$: C, 72.66; H, 11.44; N, 15.90. Found: C, 72.51; H, 11.15; N, 15.54.

[(*m*-XYL^{iPr4})Cu$_2$(CH$_3$CN)$_2$]X$_2$ (X = ClO$_4$, SbF$_6$, CF$_3$SO$_3$). To a stirred solution of 0.20 g (0.38 mmol) of *m*-XYL^{iPr4} in THF (2 mL) was added solid $[Cu(CH_3CN)_4]X$ (X = ClO_4, SbF_6, or CF_3SO_3) (0.76 mmol). Upon stirring for 10 min, the starting suspension dissolved to generate a homogeneous yellow solution, at which time Et_2O (ca. 5 mL) was added with vigorous stirring. This procedure resulted in the separation of an oily mass, which was washed several times with THF/Et_2O (1:5 v/v) and dried under vacuum to yield an off-white solid (∼0.20 g, ∼90%). The solid product thus obtained was found to be analytically and spectroscopically pure. Data for the case of X = $CF_3SO_3^-$ are as follows. ^{1}H NMR (CD_2Cl_2, 500 MHz): δ 7.59 (d, J = 7.5 Hz, 2H), 7.48−7.43 (m, 2H), 3.99 (s, 4H), 3.04 (septet, J = 6.5 Hz, 4H), 2.97−2.40 (m, 24H), 2.30 (s, 6H), 1.20 (d, J = 6.6 Hz, 12H), 1.18 (d, J = 6.5 Hz, 12H) ppm. ^{13}C{^{1}H} NMR (CD_2Cl_2, 125 MHz): δ 135.5, 134.0, 131.0, 128.5, 63.8, 57.9, 50.9, 49.2, 19.8, 19.1 ppm. ^{1}H NMR (CD_3CN, 300 MHz): δ 7.63 (d, J = 4.5 Hz, 2H), 7.44 (t, J = 7.5 Hz, 1H), 7.52 (s, 1H), 3.91 (s, 4H), 2.98 (septet, J = 6.6 Hz, 4H), 2.88−2.38 (m, 24H), 1.16 (d, J = 6.6 Hz, 12H), 1.12 (d, J = 6.6 Hz, 12H) ppm. ^{13}C{^{1}H} NMR (CD_3CN, 75 MHz): δ 135.9, 134.0, 131.1, 128.3, 63.6, 57.6, 53.6, 52.9, 50.9, 48.9, 19.4, 18.4 ppm. FTIR (KBr, cm^{-1}): 2270 (C≡N), 1263 ($CF_3SO_3^-$), 1156 ($CF_3SO_3^-$), 1031 ($CF_3SO_3^-$), 638 ($CF_3SO_3^-$). FAB-MS (MNBA), *m/z* (relative intensity, assignment): 805.4 (100, [(*m*-XYL^{iPr4})Cu$_2$(CF$_3$SO$_3$)]$^+$). Anal. Calcd for $C_{34}H_{60}N_6CuS_2O_6F_6$: C, 42.85; H, 6.35; N, 8.82. Found: C, 43.58; H, 6.12, N, 9.17.

[(*m*-XYL^{iPr4}-*d*$_8$)Cu$_2$(CH$_3$CN)$_2$](SbF$_6$)$_2$. This compound was synthesized by following the same procedure as described above for the perprotio analog. ^{1}H NMR (CD_2Cl_2, 500 MHz): δ 3.03 (septet, J = 6.5 Hz, 4H), 2.96−2.40 (m, 24H), 2.36 (s, 6H), 1.20−1.16 (two overlapping doublets, J = 6.5 Hz, 24H) ppm. ^{13}C{^{1}H} NMR (CD_2Cl_2, 125 MHz): δ 135.5, 134.0, 131.0, 128.5, 63.8, 57.9, 50.9, 49.2, 19.8, 19.1 ppm. FTIR (KBr, cm^{-1}): 2267 (C≡N), 2197 (C−D), 2159 (C−D), 2079 (C−D), 658 (SbF_6^-); FAB-MS (MNBA), *m/z* (relative intensity, assignment): 899.2 (100, [(*m*-XYL^{iPr4}-*d*$_8$)Cu$_2$(SbF$_6$)]$^+$).

[(*m*-XYL^{iPr4}-*d*$_{28}$)Cu$_2$(CH$_3$CN)$_2$](ClO$_4$)$_2$. This compound was synthesized by following the same procedure as described above for the protio analog. ^{1}H NMR (CD_2Cl_2, 300 MHz): δ 7.59 (d, J = 7.5 Hz, 2H), 7.54 (s, 1H), 7.47 (t, J = 7.5 Hz, 1H), 3.99 (s, 4H), 2.97−2.42 (m, 24H), 2.34 (s, 6H) ppm. ^{13}C{^{1}H} NMR (CD_2Cl_2, 75 MHz): δ 135.9, 134.4, 131.4, 128.8, 116.9, 64.1, 51.2, 49.6, 3.4 ppm. FTIR (KBr, cm^{-1}): 2265 (C≡N), 2225 (C−D), 2135 (C−D), 2070 (C−D), 2015 (C−D), 1092 (ClO_4^-), 623 (ClO_4^-). FAB-MS (MNBA), *m/z* (relative intensity, assignment): 783.4 (100, [(*m*-XYL^{iPr4}-*d*$_{28}$)Cu$_2$-(ClO$_4$)]$^+$).

[(*p*-XYL^{iPr4})Cu$_2$(CH$_3$CN)$_2$](ClO$_4$)$_2$. $[Cu(CH_3CN)_4]ClO_4$ (0.25 g, 0.76 mmol) and *p*-XYL^{iPr4} (0.20 g, 0.38 mmol) were mixed in THF, and the product was isolated in a manner similar to that described above for the dicopper(I) complexes of the *m*-XYL^{iPr4} ligand. ^{1}H NMR (CD_3CN, 300 MHz): δ 7.59 (s, br, 4H), 3.95 (s, 4H), 3.07−2.38 (m, 28H), 1.18 (d, J = 6.6 Hz, 12H), 1.15 (d, J = 6.6 Hz, 12H) ppm. ^{13}C{^{1}H} NMR (CD_3CN, 75 MHz): δ 135.9, 131.3, 63.3, 57.7, 53.5, 50.9, 49.1, 19.6, 18.6 ppm. FTIR (KBr, cm^{-1}): 2267 (C≡N), 1090 (ClO_4^-), 624 (ClO_4^-). Anal. Calcd for $C_{40}H_{74}N_8Cu_2Cl_2O_8$: C, 47.70; H, 7.41; N, 11.13. Found: C, 47.62; H, 7.11; N, 11.00.

[(*m*-XYL^{iPr4})Cu$_2$(CO)$_2$]X$_2$ (X = ClO$_4$, CF$_3$SO$_3$). Solid [(*m*-XYL^{iPr4})Cu$_2$(CH$_3$CN)$_2$]X$_2$ (X = ClO_4 or CF_3SO_3) (0.10 mmol) was dissolved in THF (5 mL) in a Schlenk flask. Carbon monoxide was then bubbled through the solution for 10 min at room temperature. Addition of Et_2O (5 mL) to the colorless solution yielded a white precipitate, which was recrystallized from CH_2Cl_2/Et_2O (0.09 g, ∼90%). Data for the case of X = ClO_4^- are as follows. ^{1}H NMR (CD_2Cl_2, 300 MHz): δ 7.81 (s, 1H), 7.49−7.45 (m, 3H), 4.22 (s, 4H), 3.30−3.12 (m, 8H), 3.03−2.61 (m, 20H), 1.25−1.22 (two overlapping doublets, J = 6.6 Hz, 24H) ppm. ^{13}C{^{1}H} NMR (CD_2Cl_2, 75 MHz): δ 135.6, 135.2, 132.1, 129.2, 63.7, 59.3, 53.9, 51.6, 50.6, 20.3, 20.1 ppm. FTIR (KBr, cm^{-1}): 2079 (CO), 1091 (ClO_4^-), 623 (ClO_4^-). Anal. Calcd for $C_{34}H_{60}N_6Cu_2Cl_2O_{10}$: C, 44.83; H, 6.64; N, 9.23. Found: C, 45.12; H, 6.53; N, 9.41.

Low-Temperature Oxygenation of [(*m*-XYL^{iPr4}-*d*$_x$)Cu$_2$(CH$_3$CN)$_2$](X)$_2$ (*x* = 0, 8, 28; X = ClO$_4^-$, SbF$_6^-$, CF$_3$SO$_3^-$). Solid [(*m*-XYL^{iPr4}-d_x)$Cu_2(CH_3CN)_2$](X)$_2$ was dissolved in dry CH_2Cl_2, acetone, or THF in a Schlenk flask to give solutions of varying concentrations (0.1−10 mM). These solutions were cooled to −80 °C, and dry dioxygen was bubbled through for ∼10 min. The initially colorless solutions became deep orange-to-red brown. Spectroscopic characterization was performed at a low temperature (∼−80 °C) immediately after oxygenation. Data for CH_2Cl_2 solutions at concentrations ≥2.0 mM: EPR (CH_2Cl_2, 9.4 GHz, 77 K) silent; UV−vis (CH_2Cl_2, concentration = 2.0 mM, −80 °C) (λ_{max}, nm (ϵ, M^{-1} cm^{-1})) 430 (15 000), 320 (13 000); resonance Raman (λ_{ex} = 457.9 nm, frozen CH_2Cl_2, concentration = 10 mM, 77 K) 595 cm^{-1} (^{18}O, 570 cm^{-1}); electrospray MS (CH_2Cl_2, ∼−80 °C) *m/z* (relative intensity) (*x* = 8, X = ClO_4^-) 1690.5 ({[(*m*-XYL^{iPr4}-*d*$_8$)Cu$_2$(*μ*-O)$_2$]$_2$(ClO$_4$)$_3$}$^+$, 20), 976 (100). Data for CH_2Cl_2 or acetone solutions at concentrations ≤0.1 mM: UV−vis (CH_2Cl_2, −80 °C) (λ_{max}, nm (ϵ, M^{-1} cm^{-1})): 410 (9000), 366 (15 000), 320 (8000); UV−vis (acetone, −80 °C) 410 (8000), 366 (15 500).

Low-Temperature Oxygenation of [(*p*-XYL^{iPr4})Cu$_2$(CH$_3$CN)$_2$](ClO$_4$)$_2$. According to procedures similar to those described for *m*-XYL^{iPr4} analogues, CH_2Cl_2, acetone, or THF solutions were cooled to −80 °C and dry dioxygen was bubbled through for ∼10 min. The initially colorless solutions became deep orange-to-red brown. Spectroscopic characterization was performed at a low temperature (∼−80 °C) immediately after oxygenation. Data for CH_2Cl_2 solutions at concentrations ≥2.0 mM: EPR (CH_2Cl_2, 9.4 GHz, 77 K) silent; UV−vis (CH_2Cl_2, concentration = 1.8 mM, −80 °C) (λ_{max}, nm (ϵ, M^{-1} cm^{-1})) 430 (14 000), 320 (13 000); resonance Raman (λ_{ex} = 457.9 nm, CH_2Cl_2, concentration = 8 mM, 77 K) 594 cm^{-1} (^{18}O, 570 cm^{-1}). Data for CH_2Cl_2 solutions at concentrations ≤0.1 mM: UV−vis (CH_2Cl_2, −80 °C) (λ_{max}, nm (ϵ, M^{-1} cm^{-1})) 430 (14 000), 320 (13 000).

[(*m*-XYL^{iPr4}-O)Cu$_2$(*μ*-OH)](SbF$_6$)$_2$. In a 500 mL Schlenk flask, 0.08 g (0.066 mmol) of [(*m*-XYL^{iPr4})Cu$_2$(CH$_3$CN)$_2$](SbF$_6$)$_2$ was dissolved in CH_2Cl_2 (400 mL) in a N_2 atmosphere glovebox. The solution was then exposed to an atmosphere of dry oxygen for 30 min at room temperature. The color of the solution changed from light yellow to bright green. The solvent was removed by rotary evaporation, the green residue was dissolved in THF (2 mL), and the mixture was filtered. The clear green filtrate was then carefully layered with Et_2O and stored at −80 °C. After ∼1 week, clusters of green crystals appeared and were collected and dried in vacuum to give 0.04 g (55%) of a green powder. X-ray-quality crystals were grown in a similar way except that the green THF solution was layered with Et_2O in an NMR tube. FTIR (KBr, cm^{-1}): 3632 (OH), 658 (SbF_6^-). UV−vis (CH_2Cl_2) (λ_{max}, nm (ϵ, M^{-1} cm^{-1})): 680 (200), 380 (3000), 274 (10 700). FAB-MS (MNBA), *m/z* (relative intensity, assignment): 921.3 (45, [(*m*-XYL^{iPr4}-O)Cu$_2$(OH)(SbF$_6$)]$^+$), 394 (100). Anal. Calcd for $C_{32}H_{60}N_6Cu_2O_2Sb_2F_{12}$: C, 33.21; H, 5.27; N, 7.27. Found: C, 33.14; H, 5.30; N, 7.24.

Isolation of Ligands from the Decomposition of the Bis(*μ*-oxo)dicopper Complexes. The following procedure for the *m*-XYL^{iPr4} case is representative of those used for all the ligand systems. The complex [(*m*-XYL^{iPr4})Cu$_2$(CH$_3$CN)$_2$](SbF$_6$)$_2$ (0.07 g, 0.06 mmol) in CH_2Cl_2 (5 mL) was oxygenated at −80 °C as described above. Excess O_2 was removed by bubbling N_2 through the solution for 10 min at −80 °C. The orange-brown solution then was allowed to warm to room temperature, resulting in a color change to green. An equal volume of concentrated aqueous NH_4OH was added to the green solution, and the mixture was stirred vigorously for 2−3 min, giving a deep blue aqueous and a light yellow CH_2Cl_2 layer. The aqueous layer was separated from the mixture and further extracted with 5 mL of CH_2Cl_2. The organic extracts were combined, and the above ammonia treatment and extraction were repeated two additional times. The final

CH_2Cl_2 solution was dried over $MgSO_4$ and the solvent was removed in vacuo, giving an oily yellow product. Characterization of this product by ^1H and ^{13}C NMR spectroscopy showed it to be ~3:2 mixture of *m*-XYL^{iPr4} and *m*-XYL^{iPr3H} (0.03 g, 95% mass recovery). Data for *m*-XYL^{iPr3H} are as follows. ^1H NMR ($CDCl_3$, 300 MHz): δ 7.33−7.22 (m, 4H), 3.69 (s, 4H), 2.95−2.40 (m, 27H), 1.00 (d, J = 6.6 Hz, 6H), 0.95 (d, J = 6.6 Hz, 12H) ppm. $^{13}C\{^1H\}$ NMR ($CDCl_3$, 75 MHz): δ 129.5, 127.9, 127.3, 61.7, 55.2, 54.8, 53.0, 52.6, 48.6, 47.2, 46.7, 18.7, 18.4 ppm. The presence of both *m*-XYL^{iPr4} and *m*-XYL^{iPr3H} as a mixture was further confirmed by adding a pure sample of *m*-XYL^{iPr4} to this mixture in the NMR tube; resonances due to *m*-XYL^{iPr4} gained intensity whereas resonances due to *m*-XYL^{iPr3H} remained undisturbed.

Ligand isolations from the decomposed solutions of the bis(μ-oxo)-dicopper complexes supported by *m*-XYL^{iPr4}-d_8, *m*-XYL^{iPr4}-d_{28}, and *p*-XYL^{iPr4} were performed similarly. For *m*-XYL^{iPr4}-d_8 as ligand, a mixture of 60% *m*-XYL^{iPr4}-d_8 and 40% *m*-XYL^{iPr3H}-d_8 was identified. Data for *m*-XYL^{iPr3H}-d_8 follow. ^1H NMR ($CDCl_3$, 300 MHz): δ 2.93−2.40 (m, 24H), 1.01 (d, J = 6.6 Hz, 6H), 0.96 (d, J = 6.6 Hz, 12H) ppm. $^{13}C\{^1H\}$ NMR ($CDCl_3$, 75 MHz): δ 55.1, 54.8, 53.0, 52.4, 48.5, 47.0, 46.7 ppm. For *m*-XYL^{iPr4}-d_{28} as ligand, a mixture of ~55% *m*-XYL^{iPr4}-d_8, ~30% *m*-XYL^{iPr3H}-d_8, and ~15% (*i*-Pr-d_7)$_2$ ($CH_2C_6H_4$-CHO)TACN (minus the (*i*-Pr-d_7)$_2$TACN moiety) was identified. *m*-XYL^{iPr3H}-d_{28}: ^1H NMR ($CDCl_3$, 300 MHz): δ 7.28−7.22 (m, 4H), 3.69 (s, 4H), 2.92−2.41 (m, 24H) ppm. (*i*-Pr-d_7)$_2$($CH_2C_6H_4CHO$)-TACN ^1H NMR ($CDCl_3$, 300 MHz): δ 10.0 (s, 1H), 7.88−7.33 (m, 4H), 3.74 (s, 2H), 2.92−2.41 (m, 12H) ppm. GC-MS analysis of this mixture further confirms the presence of (*i*-Pr-d_7)$_2$TACN (t_R = 9.40 min; *m/z* (relative intensity, assignment) 227 (1, M^+), 93 (100)) and (*i*-Pr-d_7)$_2$($CH_2C_6H_4CHO$)TACN (t_R = 14.55 min; *m/z* (relative intensity, assignment) 345 (1, M^+), 240 (100)). For *p*-XYL^{iPr4} as ligand, a 3:2 mixture of *p*-XYL^{iPr4} and *p*-XYL^{iPr3H} was identified. ^1H NMR ($CDCl_3$, 300 MHz): δ 7.28 (s, br, 4H), 3.63 (s, 4H), 2.95−2.82 (m, 12H), 2.61 (s, 16H), 0.94 (d, J = 6.6 Hz, 24H) ppm. $^{13}C\{^1H\}$ NMR ($CDCl_3$, 75 MHz): δ 138.9, 128.7, 62.1, 55.3, 54.8, 52.7, 52.4, 18.5 ppm.

X-ray Crystal Structure of [(*m*-XYL^{iPr4})$Cu_2(CO)_2$]$(CF_3SO_3)_2$·-$2CH_2Cl_2$. A colorless irregular-shaped crystal of the compound (grown by diffusing Et_2O into a CH_2Cl_2 solution) was attached to a glass fiber and mounted on the Siemens SMART system for data collection at 173(2) K. An initial set of cell constants was calculated from reflections harvested from three sets of 20 frames. These initial sets of frames were oriented such that orthogonal wedges of reciprocal space were surveyed; orientation matrices were determined from 235 reflections. Final cell constants were calculated from 5968 reflections from the actual data collection. Three major swaths of frames were collected with 0.30° steps in ω. A semiempirical absorption correction afforded minimum and maximum transmission factors of 0.853 and 1.000, respectively. See Table 2 for additional crystal and refinement information. The space group $P2_1/c$ was determined on the basis of systematic absences and intensity statistics. A successful direct-method solution was calculated, which provided most non-hydrogen atoms from the *E* map. Several full-matrix least-squares/difference Fourier cycles were performed, which located the remainder of the non-hydrogen atoms. All non-hydrogen atoms were refined with anisotropic displacement parameters, and all hydrogen atoms were placed in ideal positions and were refined as riding atoms with individual isotropic displacement parameters. A drawing of the cation appears in Figure 1, and selected bond lengths and angles are presented in Table 1. Full details of the structure determination, including tables of bond lengths and angles, atomic positional parameters, and final thermal parameters for non-hydrogen atoms, are given in the Supporting Information. All calculations were performed using SGI INDY R4400-SC and Pentium computers with the SHELXTL-Plus V5.0 program suite.

Acknowledgment. Funding to support this work was provided by the National Institutes of Health (Grant GM47365 to W.B.T. and Grant GM33162 to L.Q.), the National Science Foundation (NYI Award to W.B.T. and Grant CHE-9413114 for purchase of the Siemens SMART system), the Alfred P. Sloan and Camille & Henry Dreyfus Foundations (fellowships to W.B.T.), and the Swiss National Science Foundation (Grant 2000-045408.95/1 to A.D.Z.).

Supporting Information Available: Text presenting complete details of the X-ray structure determination, tables listing X-ray experimental details, positional and thermal parameters, bond distances, bond angles, and torsion angles, fully labeled ORTEP diagrams, sample Eyring plots of the individual rate constants, and a representative plot of normalized absorbances as a function of time (24 pages). See any current masthead page for ordering information.

IC970718O